HHS Public Access

Author manuscript

Nat Catal. Author manuscript; available in PMC 2023 April 19.

Published in final edited form as:

Nat Catal. 2022 October ; 5(10): 952–967. doi:10.1038/s41929-022-00856-6.

Bypassing evolutionary dead ends and switching the rate-limiting step of a human immunotherapeutic enzyme

John Blazeck[1], **Christos S. Karamitros**[1], **Kyle Ford**[1], **Catrina Somody**[1], **Ahlam Qerqez**[1], **Kyle Murray**[2], **Nathaniel T. Burkholder**[3], **Nicholas Marshall**[1], **Anirudh Sivakumar**[1], **Wei-Cheng Lu**[1], **Bing Tan**[1], **Candice Lamb**[1], **Yuri Tanno**[1], **Menna Y. Siddiqui**[1], **Norah Ashoura**[3], **Silvia Coma**[4], **Xiaoyan M. Zhang**[4], **Karen McGovern**[4], **Yoichi Kumada**[5], **Yan Jessie Zhang**[3,6], **Mark Manfredi**[4], **Kenneth A. Johnson**[3], **Sheena D'Arcy**[2], **Everett Stone**[3,6,7], **George Georgiou**[1,3,6,7,8]

[1]Department of Chemical Engineering, University of Texas at Austin (UT Austin), Austin, Texas, USA

[2]Department of Chemistry and Biochemistry, The University of Texas at Dallas, Richardson, Texas, USA

[3]Department of Molecular Biosciences, University of Texas at Austin (UT Austin), Austin, Texas, USA

[4]Ikena Oncology, Cambridge, Massachusetts, USA

[5]Department of Molecular Chemistry and Engineering, Kyoto Institute of Technology, Kyoto, Japan

[6]Institute for Cellular and Molecular Biology, The University of Texas at Austin (UT Austin), Austin, Texas, USA

[7]Department of Oncology, University of Texas Dell Medical School, LiveSTRONG Cancer Institutes, Austin, Texas, USA

Corresponding authors: John Blazeck: john.blazeck@chbe.gatech.edu, Christos S. Karamitros: karamitroschristos@gmail.com, George Georgiou: gg@che.utexas.edu.

Current addresses

School of Chemical and Biomolecular Engineering, Georgia Institute of Technology, Atlanta, Georgia, USA, John Blazeck

Aeglea BioTherapeutics, Austin, Texas, USA, Christos S. Karamitros

Trajan Scientific America's, Inc. Boston, Massachusetts, USA, Kyle Murray

Elevate Bio, Waltham, Massachusetts, USA, Norah Ashoura

Verastem Oncology, Needham, Massachusetts, USA, Silvia Coma

These authors contributed equally: John Blazeck, Christos S. Karamitros

Author Contributions

J.B., C.S.K., K.F., A.Q., C.S., N.M., A.S., B.T., W.-C.L., M.S.Y., and N.A. designed and performed directed evolution experiments and KYNase enzyme characterizations; C.S.K. and K.A.J. designed and performed pre-steady state kinetic experiments; N.T.B and Y.J.Z designed and performed crystallization experiments; C.S.K., K.M., and S.D. designed and performed HDX experiments; Y.K., C.L., Y.T., C.S.K., J.B., and C.S. expressed and prepared enzymes for *in vivo* and stopped-flow kinetic studies; S.C., M.M., X.M.Z., and K.M. designed and performed *in vivo* experiments; J.B., C.S.K., G.G., E.S., K.A.J., S.D., and Y.J.Z. interpreted the data; and C.S.K., G.G., and J.B. wrote the manuscript

Competing interests

J.B., C.S.K., N.M., W.C.L., G.G., and E.S. are inventors on intellectual property related to this work, including the active patent US9975959B2 and the pending patents US20190350975A1 and US20210207110A1, which are assigned to the Board of Regents of the University of Texas System. G.G., E.S., X.M.Z., K.M., S.C., and M.M. have equity interest in Ikena Oncology, a company pursuing the commercial development of this technology. J.B., C.S.K., C.L., and E.S. have consulted for Ikena Oncology (previously Kyn Therapeutics). The remaining authors declare no competing interests.

[8]Department of Biomedical Engineering, University of Texas at Austin (UT Austin), Austin, TX, USA.

Abstract

The Trp metabolite kynurenine (KYN) accumulates in numerous solid tumours and mediates potent immunosuppression. Bacterial kynureninases (KYNases), which preferentially degrade kynurenine, can relieve immunosuppression in multiple cancer models, but immunogenicity concerns preclude their clinical use, while the human enzyme (HsKYNase) has very low activity for kynurenine and shows no therapeutic effect. Using fitness selections, we evolved a HsKYNase variant with 27-fold higher activity, beyond which exploration of >30 evolutionary trajectories involving the interrogation of $>10^9$ variants led to no further improvements. Introduction of two amino acid substitutions conserved in bacterial KYNases reduced enzyme fitness but potentiated rapid evolution of variants with ~500-fold improved activity and reversed substrate specificity, resulting in an enzyme capable of mediating strong anti-tumour effects in mice. Pre-steady-state kinetics revealed a switch in rate-determining step attributable to changes in both enzyme structure and conformational dynamics. Apart from its clinical significance, our work highlights how rationally designed substitutions can potentiate trajectories that overcome barriers in protein evolution.

Editorial Summary:

Immunogenicity concerns preclude bacterial kynureninases for cancer immunotherapy, while the human variant lacks the desired therapeutic effect. Now, a human kynureninase enzyme was evolved to reach the activity and substrate specificity of its bacterial counterpart.

Graphical Abstract

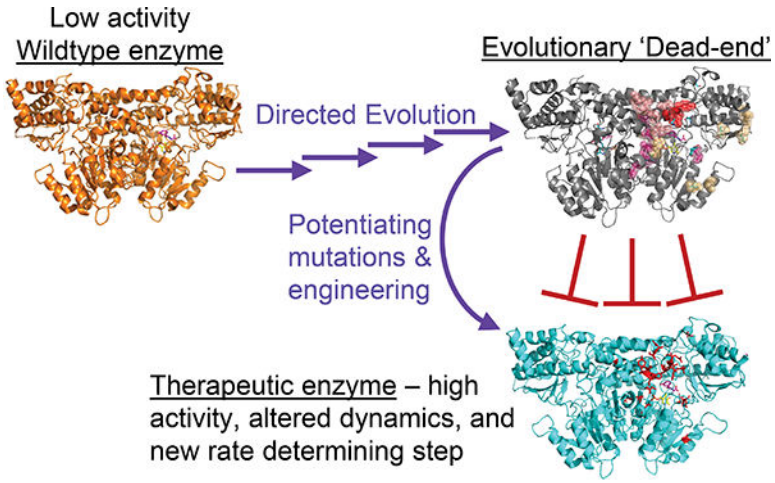

Introduction

In numerous cancers, increased Tryptophan (Trp) catabolism via indoleamine 2,3-dioxygenase (IDO1) and/or tryptophan 2,3-dioxygenase (TDO) results in accumulation of L-kynurenine (KYN) in the tumour microenvironment[1,2,3]. Elevated concentrations

of KYN and its downstream metabolites exert a potent immunosuppressive effect on lymphocytes and myeloid cells and strongly correlate with poor clinical outcomes, as well as increased resistance to immunotherapy[4,5,6,7]. The pharmacological ablation of KYN accumulation in tumours has attracted very significant interest that in turn has led to multi-billion-dollar efforts aimed at the development of small molecule drugs that inhibit IDO1[8]. Unfortunately, clinical results with IDO1 inhibitors have been disappointing in part because of sub-optimal pharmacodynamics of the tested inhibitors and additionally, because in tumours the action of TDO, in addition to IDO1, contributes to increased tumoral KYN concentrations[9]. Therefore, different approaches for achieving deep and sustained reduction of KYN levels in humans for cancer therapy are urgently needed[8,10,11,12,13]. We recently showed that administration of bacterial KYN-hydrolysing enzymes that had been conjugated to polyethylene glycol (PEG) to confer long circulation persistence are capable of complete depletion of circulating and tumoral KYN without affecting serum Trp. Enzyme-mediated depletion of KYN reversed immunosuppression in the tumour microenvironment in preclinical models, resulting in enhanced infiltration by cytotoxic T cell lymphocytes and reduced tumour growth as monotherapy, while enzyme treatment combined with immune checkpoint inhibitor (anti-PD-1 or anti-CTLA4) antibodies led to complete tumour ablation and long term T cell immunity[14].

Kynureninases (KYNases) hydrolyse the C_β-C_γ bond of KYN or 3'-OH-L-kynurenine (OH-KYN) to yield L-alanine (ALA) and either anthranilic acid (AA) or 3'-OH-anthranilic acid (OH-AA) (Fig. 1a). KYNases are pyridoxal-5'-phosphate (PLP)-dependent enzymes, and many prokaryotic and archaeal KYNases are proficient in the hydrolysis of KYN, with the extensively studied enzyme from *Pseudomonas fluorescens* (PfKYNase) having $(k_{cat}/K_M)_{KYN}$ in the ~7×10^4 M^{-1} s^{-1} range and a strong preference for KYN hydrolysis over OH-KYN hydrolysis [$(k_{cat}/K_M)_{KYN}/(k_{cat}/K_M)_{OH\text{-}KYN}$=50]. In contrast, human, and for that matter all vertebrate KYNases, have a strong preference for the hydrolysis of OH-KYN. Specifically, the human enzyme (*Homo sapiens*, HsKYNase) has reversed substrate specificity [$(k_{cat}/K_M)_{KYN}/(k_{cat}/K_M)_{OH\text{-}KYN}$ = 0.0022] relative to bacterial enzymes and poorly hydrolyses KYN with a $(k_{cat}/K_M)_{KYN}$ of only 110 M^{-1} s^{-1} [15].

In animal models, the administration of high activity, KYN-preferring, bacterial enzymes is capable of mediating a reduction of KYN levels in plasma and in tumours resulting in the reversal of immunosuppression and strong anti-tumour effects in multiple syngeneic murine cancer models[14]. In contrast, administration of the OH-KYN preferring, HsKYNase enzyme has no such effects. Unfortunately, bacterial enzymes are recognized as foreign by the human immune system, preventing their use for therapeutic applications in humans [16,17]. This is an especially important consideration for a therapeutic approach whose intended mechanism of action is to stimulate immune responses that, in turn, may promote elicitation of antibodies to foreign, i.e., non-human proteins. Thus, for clinical development it is critical to deploy a variant of the human KYNase having kinetics comparable to those of the *Pseudomonas fluorescens* enzyme to enable therapeutically meaningful depletion of circulating KYN with minimal risk of immunogenicity.

Close examination of the evolutionary and mechanistic differences among KYN and OH-KYN-selective enzymes underscore the barriers to engineering a HsKYNase variant having

high catalytic activity towards its non-preferred substrate. KYN-preferring prokaryotic enzymes and OH-KYN-preferring vertebrate enzymes are close structural homologues yet are divergent phylogenetically with amino acid identity <50%. The PfKYNase and HsKYNase have only 26% amino acid identity (45% amino acid homology), yet their aligned structures show ~1.2 Å C_α-RMSD (PDB entries: 3E9K & 1QZ9). Pre-steady state kinetic analyses showed that final product release (ALA) is the rate-determining step in the hydrolysis of their respective preferred substrates, i.e., KYN for PfKYNase and OH-KYN for HsKYNase. In contrast, a chemical step in the formation of the first product, namely AA for HsKYNase and OH-AA for PfKYNase, is rate-limiting in the catalysis of the non-preferred substrate [15]. Hydrogen-deuterium exchange mass spectrometry (HDX-MS) experiments indicated that OH-KYN hydrolysis by HsKYNase requires stabilization of its active site via hydrogen bonds with the substrate's hydroxyl group, while the bacterial enzyme does not require such active site stabilization and achieves substrate discrimination primarily by steric effects[15].

Here we show that the adaptive evolution of wild type HsKYNase (HsKYNase) for high catalytic activity towards KYN led to the isolation of an enzyme with 28x higher $(k_{cat}/K_M)_{KYN}$ catalytic activity and increased $(k_{cat}/K_M)_{OH\text{-}KYN}$. However, no further increase in KYN catalytic activity could be achieved despite the interrogation of numerous evolutionary trajectories that collectively involved the sampling of $>2\times10^9$ mutants, suggesting that this enzyme represents a dead-end or frozen intermediate. We found that the introduction of two amino acid substitutions that are phylogenetically conserved among bacterial KYN-preferring enzymes reduced the fitness of this intermediate, significantly decreasing its $(k_{cat}/K_M)_{KYN}$ without favourably affecting expression, thermodynamic stability or other protein features that have been reported to be associated with productive evolutionary trajectories, but surprisingly served to potentiate the rapid evolution of variants with high KYN activity and selectivity[18,19]. In particular, the enzyme termed HsKYNase_66, with an overall ~510x higher $(k_{cat}/K_M)_{KYN}$, fully recapitulates the catalytic and structural properties of prokaryotic KYNases. We further show that HsKYNase_66 achieves high KYN catalytic activity and selectivity via a switch in the rate-determining step of the catalytic cycle relative to parental human enzyme and that even though the kinetic properties of HsKYNase_66 closely parallel those of the bacterial KYN-preferring enzymes, the enzyme exhibits protein dynamics that are clearly distinct from those of bacterial kynureninase, as well as from the parental human enzyme. The engineering of HsKYNase_66 constitutes the critical step for the clinical development of a kynureninase variant currently in Investigational New Drug (IND)-enabling studies and which to our knowledge, will be the first immune checkpoint enzyme for cancer immunotherapy.

Results

Evolving HsKYNase using potentiating mutations to overcome evolutionary dead-ends

To enable the isolation of enzymes with increased fitness from very large libraries of HsKYNase variants (Supplementary Table 1), we first developed and validated a sensitive genetic selection. In *E. coli*, anthranilate synthetase is comprised of two polypeptide subunits, TrpE and TrpD, and catalyses the first step in the synthesis of Trp from chorismate,

producing anthranilate (AA) (Fig. 1b). *TrpE* mutants are unable to make AA and are auxotrophic for Trp. We found that an *E. coli* Δ*TrpE* strain expressing PfKYNase grew well on KYN-supplemented minimal media (lacking Trp), forming colonies after ~ 1.5 days. In contrast, cells expressing the low activity HsKYNase formed small colonies only after 4 days of incubation. *E. coli* expressing variants with 3-fold lower KYN activity (HsKYNase-H102W/N333T or HsKYNase-H102W, see Fig. 1c, d) could not support growth under these conditions. The inability of the lower catalytic activity variant to support growth was not due to impaired protein expression, as we observed comparable soluble expression yields for the wild type and the two mutant human enzymes in Trp containing media (Supplementary Table 2). We sought to assess the enzyme fitness differential that could lead to preferential enrichment of bacteria expressing higher activity enzymes in competition experiments in liquid media. After 6 serial passages (approx. 60 generations), cells expressing PfKYNase were enriched >1,000 over cells expressing the *Mucilaginibacter paludis* KYNase homologue (MpKYNase) which has ~20% lower catalytic activity ($(k_{cat}/K_M)_{KYN}$=57,000 M^{-1} s^{-1} and similar expression. The ability to enrich clones expressing proteins with relatively small differences in catalytic activity is likely because these competition experiments were performed for 6 passages resulting in selection over a high number (~60) of generations. In the lower activity regime, cells expressing HsKYNase-F306L (Supplementary Table 2, ($(k_{cat}/K_M)_{KYN}$ ~500 M^{-1} s^{-1}) were likewise enriched (i.e., >1,000 enrichment) from *E. coli* expressing HsKYNase which has 4.5-fold lower activity (and again, similar expression) after only two passages.

Ancestral sequence reconstruction (ASR) has been used successfully as a starting point for the directed evolution of many novel catalytic activities[20,21,22]. GRASP (Graphical Representation of Ancestral Sequence Predictions)[23] ancestral reconstruction with inputted phylogenetic trees for KYN- and OH-KYN-preferred KYNases obtained from the W-IQ-Tree webserver[24] revealed that the likely ancestral KYN-preferring enzyme has <67% amino acid identity to HsKYNase (Supplementary Fig. 1). In light of the high degree of sequence divergence of the ASR enzyme from the human enzyme, the putative common ancestor was not deemed to be a suitable starting point for a directed evolution campaign, given the goal of developing a high catalytic activity enzyme that is as homologous as possible to the human protein. For this reason, we selected the wild type HsKYNase as the template for directed evolution. We generated libraries of 10^7-10^8 transformants over the course of four initial rounds of directed evolution, each library constructed by a variety of approaches including random mutagenesis, structure-guided or phylogeny-guided mutagenesis of select residues, and DNA shuffling (Supplementary Table 1). Cells expressing each of these libraries were grown for 60 generations (6 passages) in selective media, as discussed above, at which point between ~100–300 clones were sub-cultured in 96-well plates and the activity of the respective variant enzymes in whole cell lysate was determined. Clones with a specific activity >20% higher than the parental species were sequenced, and the respective enzymes were produced at a preparative scale and $(k_{cat}/K_M)_{KYN}$ values determined. Four rounds of enzyme evolution yielded several variants that had around 4–5-fold higher k_{cat} and 5–6-fold lower K_M, with the most active enzyme, HsKYNase_46 having a $(k_{cat}/K_M)_{KYN}$ of 3,100 M^{-1} s^{-1} compared to 110 M^{-1} s^{-1} for HsKYNase (Fig. 1c, d). Of the nine amino acid

substitutions in HsKYNase_46 (Table 1), six were at positions at least 7 Å from the substrate binding site (Supplementary Fig. 2).

HsKYNase_46 has slightly higher catalytic activity towards OH-KYN relatively to the wild type enzyme (60,000 M^{-1} s^{-1} and 49,000 M^{-1} s^{-1}, respectively) and is a more promiscuous enzyme ($(k_{cat}/K_M)_{OH\text{-}KYN}/(k_{cat}/K_M)_{KYN}$=20 for HsKYNase_46 compared to 430 for HsKYNase; Fig. 1c, d). HsKYNase_46 has slightly better but not statistically different expression than the parental HsKYNase and both have high thermal stabilities with T_m ~ 75.85 ± 0.28 °C and 70.40 ± 0.45 °C for HsKYNase and HsKYNase_46, respectively, as determined by differential scanning fluorimetry (Supplementary Table 2). Enzyme variants that are catalytically promiscuous and/or having good stability and expression have been found to be advantageous as a template for the evolution of an improved function in numerous studies[25,18,26,27,28,29,30]. However, in this case, very extensive efforts involving the screening of libraries encompassing collectively >2×10^9 clones constructed from HsKYNase_46 by various random mutagenesis, structure-guided, or Rosetta-assisted computational protein design (in collaboration with Arzeda Inc. https://www.arzeda.com/) approaches failed to yield variants with higher catalytic activity (Supplementary Tables 1 & 2, Fig. 1e). Notably, no variants with improved catalytic activity could be isolated from a scanning saturation mutagenesis library of every individual amino acid in HsKYNase_46 (a Pfunkel library)[31]. We also generated combinatorial libraries encompassing a large fraction of all possible pairwise amino acid substitutions, constructed either by conventional DNA shuffling of the Pfunkel library or by using the RATCHIT approach which favors recombination of near neighbouring positions[32]. Again, no single or double amino acid substitutions that confer higher activity could be selected. Likewise, the screening of libraries created by: random mutagenesis of HsKYNase_46 via libraries generated by error prone PCR at different mutation rates, DNA shuffling with variants from prior rounds of evolution, libraries based on phylogenetic analysis whereby non-strictly conserved residues near the active site (within 7 Å of the H102 and N333 residues) were mutated to amino acids found in high activity KYN-preferring bacterial variants, or libraries encompassing extensive focused mutagenesis of the active site residues selected based on structural and phylogenetic considerations, again failed to yield any activity improvements (Fig. 1e, Supplementary Tables 1 and 2). We further constructed random mutagenesis libraries of HsKYNase_46 and performed neutral genetic selections in an attempt to generate an altered starting point for further evolution in a manner analogous to what had been reported in the pioneering studies by the late Dan Tawfik and his coworkers[33]. Briefly, we used cycles of low error-rate whole gene random mutagenesis coupled with reduced selective stringency by a reduced number of passages (3 passages/~30 generations instead of 6 passages/~60 generations) and periodic supplementation with 10x higher KYN concentration in the growth media which we showed independently to reduce the stringency of selection. However, no improved variants were obtained using multiple pools of clones that arose after neutral drift selection, subsequent DNA shuffling and/or additional error mutagenesis followed by purifying selection. Finally, in a further effort to explore the effect of altered selective pressure, we developed a selection for KYN-hydrolysis activity in a different host, namely complementation of a TRP1-deletion *Saccharomyces cerevisiae* strain, screening an HsKYNase_46 random mutagenesis library but again with no success. In all, these results support the notion that despite employing

a wide variety of directed evolution strategies that had proven successful in numerous earlier enzyme engineering campaigns in the literature, it was not possible to improve the catalytic properties of HsKYNase_46, establishing that this enzyme represents an evolutionary dead-end or functionally frozen enzyme with no direct trajectory to enhanced KYN activity[34,35,19].

Earlier elegant biochemical studies by Phillips and co-workers have revealed that a H102/N333 motif in the active site of HsKYNase helps coordinate the OH-KYN substrate through interactions between its aromatic ring and hydroxyl group with H102 (π-stacking interactions) and N333 (hydrogen-bond), respectively[36]. All KYN-preferring bacterial enzymes have Trp and Thr respectively at these positions. A H102W/N333T substitution in HsKYNase (HsKYNase-H102W/N333T) completely abolished the hydrolysis of OH-KYN (Fig. 1d). With KYN as the substrate, introduction of the H102W/N333T amino acid substitutions resulted in a 3-fold reduction in k_{cat}, with the K_M essentially unaffected (Fig. 1d). Stopped flow pre-steady state kinetic analysis showed that the chemical step, i.e., formation of the first product, AA, is rate-determining in the hydrolysis of KYN by HsKYNase-H102W/N333T, as is the case for the wild type human enzyme (Supplementary Fig. 3, reaction rate: 0.0007 s^{-1} ± 0.00003). In light of the phylogenetic conservation of 102W and 333T among KYN preferring enzymes and their role in substrate selectivity for KYN over its hydroxylated counterpart, we reasoned that despite their effect in reducing catalytic activity and enzyme fitness, HsKYNase-H102W/N333T may constitute a more favourable template for priming the evolution of high KYN activity. However, as mentioned above, HsKYNase-H102W/N333T failed to support growth of *E. coli* Δ*TrpE* on minimal media with KYN, either in liquid media or on agar plates, and hence fitness selections with this template were not feasible. Additionally, 96-well plate screening of saturation mutagenesis libraries, without prior genetic selection, failed to identify catalytically improved variants relative to HsKYNase-H102W/N333T parental species. Therefore, to enable fitness selections on selective media plates, the H102W/N333T substitutions were introduced into the more active HsKYNase_46 variant. This enzyme (HsKYNase_46-H102W/N333T) has a $(k_{cat}/K_M)_{KYN}$ of 210 M^{-1} s^{-1}, ~15-fold less than the parental HsKYNase_46, but importantly, ~2-fold higher relative to the wild type HsKYNase (Fig. 1c, d). HsKYNase_46-H102W/N333T could support growth in both liquid selective media and on agar plates, thus enabling fitness selections to be carried out.

With HsKYNase_46-H102W/N333T as a starting point, mutagenesis targeting residues nearby the H102W/N333T dyad and fitness selection led to the isolation of a variant, HsKYNase_64, with ~30-fold higher activity for KYN (Fig. 1c–f, Supplementary Fig. 2, Table 1). A second and similarly designed round of targeted mutagenesis and screening resulted in the isolation of several variants with further increases in $(k_{cat}/K_M)_{KYN}$ (Fig. 1c, f, Supplementary Tables 1 & 2, Supplementary Fig. 2). The highest activity variant, HsKYNase_66, catalyses the hydrolysis of KYN with very similar kinetics to those of the human enzyme for its preferred substrate OH-KYN (Fig. 1d, f) (HsKYNase_66: $(k_{cat}/K_M)_{KYN}$=56,000 M^{-1} s^{-1}, HsKYNase: $(k_{cat}/K_M)_{OH\text{-}KYN}$=49,000 M^{-1} s^{-1}). HsKYNase_66 has the reverse substrate selectivity relative to the wild type human enzyme, strongly preferring KYN over OH-KYN (Fig. 1f). Hence, in terms of catalytic activity and selectivity, this human variant is very similar to PfKYNase and other high activity, bacterial

KYN-preferring enzymes[14]. Further mutagenesis of active site loops within high activity HsKYNase variants did not yield variants with improved activity (Supplementary Tables 1 & 2). We note that in a separate experiment we employed the exact mutagenesis and selection scheme employed with HsKYNase_46-H102W/N333T that yielded HsKYNase_64, instead using the "dead-end" intermediate HsKYNase_46 as template. This effort failed to give any improved variants, once more underscoring the critical role of the H102W/N333T potentiating mutations.

The W102/T333 motif that was critical for potentiating the evolution of HsKYNase_66 plays a key role in dictating substrate selectivity. Reversion of Trp102 to His or of Thr333 to Asn reduced its catalytic activity for KYN by 12- and 7-fold, respectively. Similar to HsKYNase_66, both HsKYNase_66-W102H and HsKYNase_66-T333N preferentially hydrolyse KYN over OH-KYN, with $(k_{cat}/K_M)_{KYN}/(k_{cat}/K_M)_{OH\text{-}KYN}$ ratios of 15 and 18, respectively. By contrast, in combination the W102H/T333N reversion resulted in a dramatic >30-fold increase in $(k_{cat}/K_M)_{OH\text{-}KYN}$. As a result, HsKYNase_66-W102H/T333N acquires inverse substrate selectivity relative to its parental enzyme, preferentially hydrolysing OH-KYN with a (k_{cat}/K_M) that is comparable (<2-fold lower) to that of the native human enzyme (Fig. 1f). This finding is consistent with the proposed critical role of H102 and N333 in coordinating the hydroxyl group of OH-KYN for efficient catalysis. The W102H and T333N mutations exhibit a strong reciprocal sign epistasis effect since they individually impair the OH-KYN activity of HsKYNase_66, whereas in combination they are highly beneficial. Reciprocal sign epistasis is associated with very rugged fitness landscapes[37–39] and is in line with the absence of a direct evolutionary trajectory from the parental wild type HsKYNase enzyme to HsKYNase_66. Underscoring the complexity of the fitness landscape, the synergistic effect of these two potentiating substitutions (H102W/N333T) on $(k_{cat}/K_M)_{KYN}$ is highly dependent on the mutational background of the parental species, showing a higher-order positive sign epistasis[40] as described in Supplementary Fig. 4 (ratios of H102W/N333T mutational effect on intermediate evolved species/effect on HsKYNase were ~ 0.23 for HsKYNase_46 and 21 for HsKYNase_66).

Pre-Steady-State kinetics reveal altered rate-limiting step

Pre-steady state kinetic analyses were performed by monitoring the fluorescence of the first product, anthranilate (AA) or hydroxy-anthranilate (OH-AA) in the msec regime using a stopped-flow apparatus. In the reaction of HsKYNase with its non-preferred substrate, KYN, AA accumulation was linear over time, indicating that the rate-limiting step is the chemical reaction (or a step that precedes it) leading to AA formation (Fig. 1a, 2a)[15]. Fitting the pre-steady state data to a single exponential burst model, we estimated a steady-state rate of 0.04±0.003 s^{-1} which is in close agreement with the v/[E] steady-state rate measured at the same KYN concentration (v/[E] ~ 0.06 s^{-1} at 800 mM KYN). In contrast with HsKYNase_66 and KYN, we observed a distinct AA burst phase with a decay rate (eigenvalue) of 38.6 ± 1 s^{-1} during the first 50 msec of the reaction which was then followed by a linear phase with a steady-state rate of 1.25 ± 0.05 s^{-1} (Fig. 2b). Since the k_{cat} at steady state is ~ 1.5 s^{-1}, it follows that a step after the formation of AA, possibly corresponding to the release of the ALA product, is rate-limiting. Thus, in the evolution of HsKYNase_66 from the parental human enzyme, the rate-determining step was switched

from AA formation in the case of the parental enzyme to product release for the high KYN activity evolved human variant. In HsKYNase_66, the rate of AA formation was accelerated at least 600-fold (38.6/0.06). Of note, product release is the rate-determining step for the KYN-preferring PfKYNase, which shows a very similar burst decay value 32±0.6 s^{-1} and a linear, steady-state rate of 5.7±0.02 s^{-1} [15].

Similarly, product release is the rate-determining step in the reaction of the parental HsKYNase with its preferred substrate, OH-KYN (Fig. 2c). These findings demonstrate that for kynureninase enzymes having high activity and selectivity, regardless of whether their preferred substrate is KYN or its hydroxylated form (OH-KYN), the chemical step leading to the formation of the first product is rapid and therefore, the steady-state reaction rate is limited by the rates of subsequent intermediate steps that lead to release of the second product, ALA. Conversely, the chemical steps leading to the formation of either AA or OH-AA is rate-determining in the catalysis of the non-preferred substrate. This is the case for HsKYNase with KYN, PfKYNase with its non-preferred substrate OH-KYN, and HsKYNase_66 with OH-KYN [15]. As shown in Fig. 2d, for the latter, OH-AA formation is linear over time with a rate constant 0.13 ± 0.035 s^{-1}. Finally, we note that when the H102W/N333T motif was directly incorporated on HsKYNase, no change of the rate-determining step was detected while the catalytic rate was greatly diminished (reaction rate: 0.0007 s^{-1} ± 0.00003, Supplementary Fig. 3).

Structural analysis of HsKYNase_66

The structure of HsKYNase_66 was solved at 3.25 Å resolution (Fig. 3, Supplementary Figs. 5 & 6, Supplementary Table 3). The enzyme formed crystals in the $I4_122$ space group with two identical polypeptide chains in each asymmetric unit forming a dimer. The overall fold of HsKYNase_66 is almost identical to that of HsKYNase and its close structural homologue of PfKYNase (Supplementary Fig. 7). Compared to PfKYNase, the human enzymes have a loop insertion consisting of residues 50–67. In HsKYNase_66, the N67D mutation forms a salt bridge with R43, thereby stabilizing this long loop relative to the parental human enzyme. (Supplementary Fig. 8a).

In HsKYNase_66, most mutations are located at the dimer interface close to the active site pocket, clustering in a hydrophobic region that enhances the recognition of the substrate's phenyl ring (Fig. 3a, b). Near this pocket, a loop consisting of 16 residues (I97-G112) appears to have undergone a considerable conformational change (Supplementary Fig. 7d, Supplementary Fig. 8b–d). Within this loop, the H102W and E103F amino acid substitutions increase the hydrophobicity of the substrate binding pocket, and the side chain of F103 in HsKYNase_66 adapts a perpendicular conformation relative to E103 of HsKYNase and given its location, affects the shape of the substrate binding pocket (Supplementary Fig. 6a).

The substrate binding pocket of KYNases can be in open or closed conformations [36,41,42]. Substrate-free, wild type HsKYNase is in the open conformation, identifiable by the position of the R434 side chain guanidino nitrogens, which are directed away from the active site and are stabilized by a hydrogen bond network with D426, T404, and Y226 (Fig. 3c, Supplementary Fig. 9a) [41]. In the presence of the 3-OH-Hippuric acid inhibitor substrate, HsKYNase's R434 guanidino nitrogens are shifted by ~8Å, facing the active site[36]. In

this closed conformation, R434 is stabilized by hydrogen bonds with the α carboxyl of 3-OH-Hippuric acid and D426 and F225 (Fig. 3c, Supplementary Fig. 9b). Notably, substrate-free HsKYNase_66 and PfKYNase [42] are also in a closed conformation, with R434 prepositioned in the active site. The backbones of the R428-R434 loop of HsKYNase_66 and PfKYNase are also shifted compared to HsKYNase (Fig. 3c, Supplementary Fig. 9c–e).

A loop very close to the substrate binding pocket, containing the triad A280-G281-A282 (AGA) in HsKYNase is mutated to S280-S281-P282 (SSP) in the evolved variant, HsKYNase_66 (Fig. 3d, Table 1). Whereas an A(S/T)-G-A amino acid triad at positions 280–282 is highly conserved among eukaryotic enzymes (Supplementary Fig. 10), in KYN-preferring kynureninases from bacteria the structurally equivalent positions contain a strictly conserved G/S-G/S-P motif (Supplementary Fig. 11). For example, MpKYNase has an SSP motif (S248-S249-P250 in *M. paludis* sequence, Uniprot entry H1YAV1) while PfKYNase has a GGP triad (G231-G232-P233). In HsKYNase_66 and other high KYN activity enzymes, including PfKYNase, the proline residue that is near the W102 and W109 residues can further increase the local hydrophobicity of this region, which is critical for optimal interactions between the substrate's aromatic ring and W102, as discussed above. The A282P substitution is located at the turn of this loop and may restrain its flexibility as is the case with PfKYNase (Supplementary Fig. 12a, b).

Certain mutations found in HsKYNase_66 are located in proximity to the enzyme's PLP binding site (Supplementary Fig. 6b). More specifically, the introduction of a hydroxyl group at position 136 (A136T) may allow formation of a hydrogen bond (Fig. 3e, Supplementary Fig. 6b), similar to the stabilizing interaction of T96 with the phosphate group of PLP in PfKYNase (Supplementary Fig. 12c, d). On the other side of the PLP, the N333T mutation, a key contributor to substrate discrimination through the disfavouring of OH-KYN binding, could form a hydrogen bond network with Y275 and the phosphate group of the PLP (Fig. 3b, Supplementary Fig. 6) [15,36].

Conformational dynamics of HsKYNase_66 during catalysis

The conformational dynamics of HsKYNase_66 were determined in the presence and absence of KYN or OH-KYN and compared to the wild type enzyme and to PfKYNase[15]. The HDX-MS analyses of HsKYNase_66 were carried out under identical conditions as those described for HsKYNase and PfKYNase, and peptides from regions not involved in binding and/or catalysis showed similar maximum deuteration between HsKYNase_66 and HsKYNase. In HDX-MS experiments, approximately 130 overlapping peptides were analysed after 1, 10 or 100 min exposure to D_2O, and for each peptide the difference in average deuterium (D)-uptake in the presence and absence of substrate was calculated (see Supplementary Tables 4 & 5 for D-uptake data; only significant differences with p-value <0.01 and an average |ΔHDX| >0.3 were considered). Steady-state parameters of HsKYNase_66 determined in D-PBS (k_{cat}^{KYN}=0.24±0.01 s^{-1}, K_M^{KYN}=0.047±0.0055 mM and $k_{cat}^{OH\text{-}KYN}$=0.23±0.019 s^{-1}, $K_M^{OH\text{-}KYN}$ =1.37±0.2 mM) suggest that the reaction was under steady-state conditions for the first two timepoints.

Comparison of D-uptake by HsKYNase_66 in the presence and absence of KYN (Fig. 4a, c, Supplementary Fig. 13a) revealed that the region surrounding the critical H102W mutation,

which is important for KYN specificity, did not show any D-uptake difference upon addition of substrate (Fig. 4a, c, e e.g., peptide D92-F103). The nearby 2nd-shell active site region A270-I290 that includes the SSP motif, however, showed decreased D-uptake (Fig. 4a, c, e e.g., peptide W272-F289). In contrast, the parental HsKYNase showed a statistically significant stabilization of the Y100-I116 region that encompasses the critical H102 residue (only at t=10 minutes), with no changes in exchange in the A270-I290 region (Fig. 4b, d)[15]. Similar to HsKYNase, the KYN-preferring PfKYNase enzyme also has shown stabilization of the region that harbours the cognate W64 residue (only at t=10 minutes) and no change in the G231-G232-P233 region (Supplementary Fig. 14a, b). These findings suggest that the hydrophobic region in HsKYNase_66 active site (I99-W102-F103-W109) that could promote π-stacking interactions with the aromatic ring of KYN is pre-organized for efficient KYN binding and subsequent productive turnover.

A reduction in D-exchange is also observed for I218-Y226 (Fig. 4a, c, e e.g., peptide F220-T237) and R399-L403 in HsKYNase_66 upon addition of KYN (Fig. 4a, c, e e.g., peptide I390-L403). Both of these regions are involved in hydrogen bonding networks in the closed conformation of the enzyme that is observed following substrate binding by HsKYNase and, alternatively, in the resting state of HsKYNase_66 and PfKYNase (i.e., without substrate binding, Supplementary Fig. 9). I218-Y226 contains the V223I and F225Y mutations, and the Y226 hydroxyl group can hydrogen bond with either of R428's guanidino nitrogens in HsKYNase, depending on the conformation of the R428 side chain, while Q402 and T404 (contained or adjacent to the R399-L403) form hydrogen bonds with F/Y225 and Y226 backbone carbonyls (Supplementary Fig. 9a–d)[36,41,42]. The homologous loop in PfKYNase (peptide V333-Y353) showed a decrease in D-uptake in the reaction with KYN at t=10 minutes, but not with OH-KYN (Supplementary Fig. 14) [15]. Similar decreases in D-uptake were observed when the less preferred OH-KYN was added to HsKYNase_66 (Supplementary Fig. 13b, 15a, c). The conformational dynamics of both of these regions are not affected by substrate turnover (either KYN or OH-KYN) in the HsKYNase enzyme (Fig. 4b, d, Supplementary Fig. 15b, d)[15].

We observed a time-dependent increase in D-uptake in regions surrounding the PLP-cofactor and involved in the dimer interface during the catalysis of either KYN or OH-KYN by HsKYNase_66. These regions include N135-T138 (Fig. 4e e.g., peptide M134-L141), E161-N182 (Fig. 4e e.g., peptides L160-E173 and S174-N182), and H291-L338 (Fig. 4e e.g., peptides 311–329 and 329–337). N135-T138 contains the A136T mutation and is in the vicinity of the phosphate group of the PLP. E161-N182 does not contain any mutations, but F165 and D168 within this region can directly interact with the PLP cofactor. H291-L338 contains the important N333T mutation, as well as an I331C substitution, and it encompasses a long loop at the dimer interface that also interacts with the phosphate groups of PLP. The increased flexibility of N135-T138 that contains the A136T substitution is of interest considering the possible H-bond formation between T136 and the phosphate group of PLP (Fig. 3e). The extent of increased D-uptake was similar for the reaction with KYN or with OH-KYN, and in both cases the uptake appeared to increase at 10 minutes; larger increases were observed for OH-KYN after 100 minutes when the reaction is no longer predicted to be at steady state (Fig. 4e). We note that the crystal structure of HsKYNase_66 was solved in the absence of substrate, thereby reflecting the resting enzyme

state (internal aldimine), whereas HDX-MS samples solution conformational states during catalysis[43]. Importantly, the destabilization of the pocket surrounding the PLP cofactor was not observed in the wild type human (Fig. 4b, d, Supplementary Fig. 15b, d) or PfKYNase (Supplementary Fig. 14) enzymes[15] and represents a unique property of HsKYNase_66. These findings suggest that the evolution of HsKYNase_66 led to significant shifts in the conformational dynamics during catalysis, as manifested by the increased flexibility of regions in the active site and the PLP binding pocket and further by the selective stabilization of more remote regions upon substrate binding (for direct comparison of overall D-uptake by HsKYNase_66, HsKYNase and PfKYNase in the presence of KYN and OH-KYN, see Supplementary Figs. 16 & 17).

High activity HsKYNase anti-tumour activity

We next determined if a human KYNase enzyme with high $(k_{cat}/K_M)_{KYN}$ can have similar anti-tumour effects as bacterial enzymes. A variant of HsKYNase_66 named HsKYNase_95 (Table 1, Supplementary Table 2) having catalytic properties indistinguishable from HsKYNase_66 and whose KYN activity is equally dependent on the H102W/N333T potentiating mutations was expressed at a preparative level, purified to near homogeneity, confirmed to contain low endotoxin, and finally conjugated to 5 kDa PEG-NHS ester for prolonged systemic retention in circulation. HsKYNase_95 showed higher stability than HsKYNase_66 during incubation in the presence of 50% serum *in vitro*, a property that qualitatively correlates with stability in circulation in animal models, making it more suitable for *in vivo* studies (Supplementary Fig. 18). Compared to HsKYNase_66, HsKYNase_95 has an additional A68T mutation near the predicted salt bridge resulting from the N67D mutation (Supplementary Fig. 8a), two conservative substitutions, I110L and F306W, and a S274N mutation. HsKYNase_95 lacks the A132V and V223I mutations found in HsKYNase_66 (Table 1). These positions all lie within active site loops, and of note, residues 132 and 306 are near the observed area of relative destabilization along the dimer interface and PLP pocket. As we have found that loss of the PLP cofactor is a reason for the deactivation of PLP-enzymes in biological fluids, we speculate that the conservative amino acid substitutions in HsKYNase_95 at positions 132 and 306 may play a role in the favourable pharmacokinetics exhibited by this enzyme relative to HsKYNase_66. Syngeneic tumours were established in mice by injection of 5×10^4 CT26 colon carcinoma cells (which are known to express IDO1 and to accumulate KYN in the tumour microenvironment), in the right flank, and treatment was initiated when tumour size reached 50–100 mm^3. While administration of PEGylated wild type human kynureninase (i.e. PEG-HsKYNase) at 20 mg/kg weight has no effect on tumour growth in syngeneic tumour models[14], treatment with PEG-HsKYNase_95 with the identical dosing regimen significantly retarded tumour growth (Fig. 5, Supplementary Fig. 19). We further compared the effect of PEGylated HsKYNase_95 with that of an antagonistic antibody targeting PD-1, a widely used and successful immune checkpoint inhibition modality. Treatment with the PEGylated HsKYNase_95 variant retarded tumour growth to the same degree achieved by anti-PD-1 antibodies at the dose and frequency established to be optimal for this cancer model[44] (Fig. 5). No statistical difference in body weight during the course of the experiment was seen across treatment arms (Supplementary Fig. 20).

Discussion

Bacterial kynureninases have evolved to have high catalytic selectivity for KYN over OH-KYN whereas their animal orthologous enzymes exhibit the reverse selectivity and catalyse the hydrolysis of OH-KYN. The catalytic properties of prokaryotic and animal enzymes probably reflect their distinct physiological roles. In animals, Trp homeostasis is maintained by the kynurenine pathway in the liver and brain. However, under inflammatory conditions the action of IDO1 leads to the accumulation of KYN in tissues where it serves in key immune-suppressive and neuro-modulatory roles *in trans*. Presumably, the high K_M of animal kynureninases for KYN is important for preventing its consumption in inflammatory settings.

We had shown earlier that administration of PEGylated high KYN-activity bacterial kynureninases can reverse the immune suppression that arises from the tumoral production of KYN[14,45]. However, the clinical experience with the two approved PEGylated bacterial enzyme therapeutics, pegaspargase[46] and pegloticase[47], has established that in spite of PEGylation partially masking bacterial proteins from recognition by the immune system, adverse antibody responses arise in most patients after repeated administration that necessitates discontinuation of treatment. For this reason, an engineered, high KYN activity variant of the human kynureninase is required for therapeutic purposes.

The considerable degree of sequence divergence (e.g., sequence identity of 27% for *P. fluorescens* and 48% for *M. Paludis,* the KYN-preferring enzyme with the highest homology to HsKYNase), the different conformational dynamics, and the distinct rate-determining steps in the reaction with KYN (i.e., ALA release for *P. fluorescens* vs AA formation for HsKYNase), underscore the difficulty associated with switching the catalytic specificity of the human enzyme. Efforts to engineer a high KYN catalytic activity HsKYNase variant via structure-guided or directed evolution approaches, with the latter involving combinations of a highly sensitive fitness selections and 96 well plate screening, resulted in the isolation of HsKYNase_46. As discussed in the Results section (Fig. 1), very extensive efforts employing numerous approaches and evolutionary trajectories that collectively involved the functional interrogation of $>10^9$ variants did not succeed in producing variants of HsKYNase_46 with higher catalytic activity, thus providing compelling evidence that this enzyme represents a dead-end evolutionary intermediate. Having said that, we acknowledge that it is possible that technical limitations may have limited the search of the protein sequence space around HsKYNase_46, such as for example unidentified biological constrains that might have biased the genetic selection.

It was only after the introduction of two potentiating substitutions, H102W and N333T, that a facile path towards high KYN catalytic efficiency could be accessed. Trp at position 102 and Thr at 333 are phylogenetically conserved among all KYN-selective bacterial enzymes and are not found among their non-prokaryotic, OH-selective orthologs. As shown in Fig. 1d, these two substitutions completely abolish OH-KYN activity. Each of these mutations individually or in combination reduce KYN catalytic activity in HsKYNase, and therefore could not be isolated via mutation of the wild type enzyme by fitness selection alone.

However, the introduction of the deleterious H102W/N333T motif in the context of HsKYNase_46, which has 28X higher KYN activity than HsKYNase, afforded sufficient KYN hydrolysis to support growth of *E. coli* Δ*trpE* cells in selective media. In directed evolution literature, intermediates that lead to higher catalytic activity towards a desired substrate frequently show higher expression or thermodynamic stability which can be instrumental for tolerating the introduction of destabilizing epistatic mutations and/or they have expanded substrate promiscuity (i.e., generalist enzyme intermediates) [27,48,49]. This was not the case for HsKYNase_46-H102W/N333T which: has comparable stability and expression yield as its parental template, HsKYNase_46, is a *bona fide* specialist showing no activity towards OH-KYN and importantly, has 15-fold lower KYN activity and substantially lower fitness than its parental evolutionarily frozen variant, HsKYNase_46. Yet two rounds of mutagenesis of HsKYNase_46-H102W/N333T variant enabled rapid isolation of HsKYNase_66, with $(k_{cat}/K_M)_{KYN}$ comparable to the most active KYN-preferring bacterial homologs. Of note, employing the identical mutagenesis scheme and screening strategy that led from HsKYNase_46-H102W/N333T to HsKYNase_66 using HsKYNase_46 (lacking potentiating mutations) as the template failed to lead to increased catalytic activity, further underscoring the key role of these two residues. The potentiating effect of H102W/N333T is quite unusual and may be related to complex epistatic effects that prime favourable changes in protein dynamics to favor the catalysis of KYN, as well as structural modifications to mimic its bacterial high activity homologs.

The crystal structure of HsKYNase_66 suggests that the H102W substitution, along with additional mutations located in its proximity, alter the hydrophobicity and the shape of a crucial active site loop to better accommodate KYN (Fig. 3b, Supplementary Fig. 8). In addition, a large shift in HsKYNase_66's R428-R434 loop occurs as it assumes a closed conformation in which the R434 side chain is prepositioned in the active site, such that it resembles the conformation of substrate-free PfKYNase (Fig. 3c, Supplementary Fig. 9) [36,41,42]. Structural and HDX-MS data further indicate that the N333T substitution may be important for stabilizing the PLP cofactor during initiation of the KYN catalytic cycle, as well as in playing an important role in active site's conformational dynamics during catalysis. The N333T substitution increases the k_{cat} of the evolved HsKYNase_66 by 25-fold (k_{cat} of HsKYNase_66 vs k_{cat} of HsKYNase_66-T333N) while having a minor effect on the k_{cat} of the HsKYNase_46 or the wild type enzymes (Fig. 1d, f).

It is quite remarkable that HsKYNase_66 has KYN catalytic activity and KYN-vs-OH-KYN selectivity comparable to the most active bacterial enzymes known. What is more, in HsKYNase_66 the rate-determining step in the reaction with KYN was switched from AA formation as in the wild type enzyme to product release, as is the case with its bacterial orthologs (Fig. 2). To the best of our knowledge, there are very few examples where a change in the rate-determining step during the course of directed evolution has been inferred[50], let alone experimentally demonstrated by pre-steady-state kinetic analyses. Interestingly, the majority of the mutations in HsKYNase_46 are located in 2nd and 3rd shell positions (1st shell positions are defined as those residues which directly interact with substrate or PLP). Similarly, 11/13 mutations that accumulated in the evolution from HsKYNase_46-H102W/N333T to HsKYNase_66 are located in 2nd and 3rd shell positions. Interestingly, a correlation between catalytic efficiency of HsKYNase_66 toward

KYN and OH-KYN and the extent of the respective decrease in D-uptake was observed in these regions harbouring 2nd and 3rd shell mutations, further linking the role of remote mutations to catalytic activity. A large body of literature suggests that flexibility is an important component of catalysis allowing the enzyme to simultaneously sample multiple and catalytically competent conformations [51,52,53,54,55]. We further established that the introduction of the potentiating mutations alone is not sufficient to switch the rate-determining step in the hydrolysis of KYN (Supplementary Fig. 3). Therefore, the switch of the rate-limiting step and attainment of high KYN activity must be dependent on a broader subset of the amino acid substitutions that accumulated in HsKYNase_66.

Whereas all other KYN-preferring kynureninases show <50% sequence identity with eukaryotic enzymes, HsKYNase_66 and 95 are close homologues of the parental human enzyme (95% identity). Consequently, our work demonstrates that high KYN activity and selectivity can be accommodated within the primary sequence of animal enzymes. This finding raises the question of why there is such a large degree of sequence divergence between KYN and OH-KYN preferring enzymes in the natural world in the first place? Possibly selective pressure for protein features other than catalysis *per se*, perhaps relating to the different functions and regulation of KYN in the different kingdoms of life may have led to distinct evolutionary paths for KYN and OH-KYN preferring enzymes. Conceivably, the high KYN catalytic activity and specificity of HsKYNase_66, despite its largely human primary amino acid sequence, might have been co-evolved with the enzyme's conformational dynamics, predominantly through the incorporation of structural flexibility during catalysis; in a manner not previously observed in HsKYNase or in PfKYNase. The role of conformational flexibility in protein evolution has been highlighted in several previous studies[53,56,57,58,59] as a key property for the shift of the ensemble of conformational states and the respective functional transition in an evolutionary trajectory. Perhaps most importantly, in addition to the many interesting ramifications entailed in the directed evolution and catalytic properties of KYN-specific human KYNase enzymes, we have shown that such enzymes are capable of mediating a strong anti-tumour effect in a mouse tumour model, with minimal risk of future anti-drug immunogenicity because of an absence of strong T cell epitopes as determined by computational immunogenicity analysis and importantly, because conjugation to PEG impedes immune recognition [60,61]. A therapeutic, highly active, PEG-HsKYNase variant is in IND-enabling studies for future clinical evaluation in patients with advanced solid tumours (https://ir.ikenaoncology.com/news-releases/news-release-details/kyn-therapeutics-enters-global-strategic-collaboration-celgene)

Methods

HsKYNase expression vector construction

The wild type *Homo sapiens* kynureninase (HsKYNase), codon optimized for expression in *E. coli* and harbouring an N-terminal 6X histidine tag, was amplified from a previously described plasmid [14]. This amplicon was inserted into the pMAL-c2x *E. coli* expression vector in place of the maltose-binding fusion protein (MBP) using Gibson Cloning to create an ampicillin resistant vector, dubbed pMal-noMBP-wtHsKYNase, in which expression of

HsKYNase is driven by the Tac promoter [62]. A modified vector with chloramphenicol resistance, dubbed pMal-CAM, was also constructed such that a HsKYNase gene or library of variants could be inserted between XmaI and KpnI restriction enzyme sites.

E. coli cloning, enzyme expression strains, and strain construction

The *E. coli trpE* deletion mutant (strain genotype = F-,Δ(araD-araB)567, ΔlacZ4787(::rrnB-3), λ-, ΔtrpE772::kan, rph-1, Δ(rhaD-rhaB)568, hsdR514) was obtained from CGSC, *E. coli* Genetic Resources at Yale, and was thereafter referred to as K12 ΔtrpE. The ΔtrpE772::kan DNA region was transferred into the *E. coli* T7 Express strain from New England Biolabs (strain genotype = fhuA2 lacZ::T7 gene1 [lon] ompT gal sulA11 R(mcr-73::miniTn10--TetS)2 [dcm] R(zgb-210::Tn10--TetS) endA1 Δ(mcrC-mrr)114::IS10) using P1 phage transduction [63].

E. coli strains K12 ΔtrpE, Bl21(DE3), C41(DE3), C43(DE3), T7 Express (New England Biolabs), T7 ΔtrpE, and MC1061 were used for routine molecular cloning and plasmid propagation [4]. *E. coli* strains were grown at 37°C with constant shaking in Lenox LB media supplemented with 50μg/ml of ampicillin, 50μg/ml of kanamycin, or 35μg/ml of chloramphenicol as necessary.

Initially, library preparation and screening was performed in three strains as follows (1) transformation of ligated DNA into MC1061 and subsequent extraction of plasmid library DNA by miniprep, followed by (2) transformation of the library into the K12 ΔtrpE strain, selection for improved variants, followed by (3) transformation of individual plasmids into strains Bl21(DE3), C41(DE3), C43(DE3), or T7 Express for HsKYNase expression. Ultimately, the T7 ΔtrpE strain was utilized for all steps.

Cloning and transformation procedures

Restriction enzymes were purchased from New England Biolabs and used according to standard protocols. Library preparation routinely required amplification and purification of several DNA sections of the HsKYNase gene, followed by assembly mediated by KOD DNA polymerase or KOD Hotstart DNA Polymerase. PCR amplicon fragments were routinely incubated at 37°C with DpnI enzyme to eliminate plasmid template DNA. KOD-mediated assembly reactions were performed without primers and with 1μg total DNA of the DNA fragments to be assembled, normalized by molar amounts, followed by a second PCR using 5–10μl of the DNA assembly reaction as template and standard addition of primers. Primer sequences used for molecular cloning and library creation can be found in Supplementary Table 6.

Error-prone PCR of an entire HsKYNase gene was performed using Taq DNA Polymerase for 25 cycles with the following reagents in eight 20μL PCR reactions containing the following: 0.22 mM dATP, 0.20 mM dCTP, 0.27 mM dGTP, 1.88 mM dTTP, 2.75 mM $MgCl_2$, 0.5 mM $MnCl_2$, 0.005 mg/ml BSA, 20–100ng of HsKYNase plasmid DNA, and 0.5μM of primers JB68/70 (5’→3’ ‘ctcaggtaccatatgggcggtcatcatcacca’ and ‘ctgcagccgtcgacctagtttttggtttccgcactgtcc,’) or JB270/271 (5’→3’ ‘cactgtgtggtaccgaggtaatacatgggcggtcatcatcaccaccatcatgg’ and ‘cgagtcagcccgggtaatccgcggctagtttttggtttccgcactgtcca’).

HsKYNase amplified libraries were gel-purified and digested for use for library preparation as described below. Ligation reactions were performed overnight at 16°C or 22°C using T4 DNA Ligase (New England Biolabs). Transformation of *E. coli* strains was performed using standard electroporator protocols.

Introduction of the bacterial KYNase motifs (H102W and/or N333T) was performed using oligo-mediated site directed mutagenesis and Gibson assembly of overlapping fragments that contained the mutation(s) into a pMal-CAM plasmid backbone. Reversion of the bacterial KYNase motifs (W102H and/or T333N reversions) were performed similarly.

Large-scale library preparation

High efficiency library preparation was performed by ligating HsKYNase library DNA amplified by primers JB068/070 and digested with NdeI/SalI-HF/DpnI into the pMal-noMBP-HsKYNase digested with NdeI/SalI-HF or by ligating HsKYNase library DNA amplified by primers JB270/271 and digested with KpnI-HF/XmaI/DpnI into the pMal-CAM vector DNA digested with KpnI-HF/XmaI. Libraries inserted into the pMal-noMBP and pMal-CAM vector backbones were selected for with ampicillin or chloramphenicol, respectively. All ligations contained 100ng of digested HsKYNase library insert and 100ng of digested vector backbone, approximating a 3:1 molar ratio, and were performed overnight before heat deactivation.

Heat deactivated ligations were dialyzed against ultrapure water for 20 minutes prior to electroporation into freshly prepared electrocompetent cells. After electroporation, *E. coli* cells were allowed to recover at 37°C in 1mL of SOC media with shaking. After recovery, the cells were plated on LB antibiotic plates (Corning) and grown overnight at 37°C until visual confirmation of individual colonies or were grown overnight at 37°C in 25mL of LB antibiotic media.

Library size was determined by plating 0.01, 0.1, or 1μL of cells recovered in SOC and counting individual colonies. Library diversity was determined by sequencing single colonies.

Genetic selection for enhanced kynureninase variant activity

A defined culture media, dubbed M9-KYN media, was created to allow selection of higher activity HsKYNase variants harboured in *E. coli* K12 or T7 ΔtrpE cells from a pool of cells harbouring less active HsKYNase variants. M9-KYN media contained 1X Difco™ M9 minimal salts (Becton, Dickinson and Company), 2 mM magnesium sulfate (Fisher Scientific), 0.1 mM calcium chloride (Sigma Aldrich), 2% glucose (Sigma Life Sciences), 0.10 mM isopropyl β-D-1-thiogalactopyranoside (IPTG; Fisher Scientific), antibiotic (ampicillin or chloramphenicol), between 25 and 100 μM L-Kynurenine (Kyn) (Sigma Aldrich), and UltraPure water.

A generalized genetic selection process proceeded as follows. An initial inoculum of 10^5-10^{10} *E. coli* K12 or T7 ΔtrpE cells (10-fold more cells than the calculated library size) harbouring a library of HsKYNase variants was inoculated into 25mL of M9-KYN media and then grown at 37°C with shaking at 220RPM until the OD_{600} > 1.0. 1mL of the

resultant culture was washed 3X in sterile DPBS, and 20 to 50% of the initial inoculum by cell count was used to inoculated 25mL of fresh M9-KYN media and cultivated at 37°C with shaking at 220RPM until OD_{600} > 0.50. In general, six rounds of selection (inoculating with a reduced number of cells for each round) were performed for each library, prior to plating on LB antibiotic plates for further screening.

96-well assay of enzyme specific activity in cell lysate

Individual colonies of *E. coli* expressing different HsKYNase variants were picked into a 96-well U-bottomed plate containing LB + antibiotic, with controls expressing known HsKYNase variants included in quadruplicate. After overnight growth, 2μL was used to inoculate a fresh 96-well U-bottomed plate containing 70μL TB + antibiotic per well. This expression plate was grown at 37°C for 4 hours, and then kynureninase expression was induced by adding 70μL TB + antibiotic + 1mM IPTG to each well, followed by overnight induction at room temperature.

Induced cells were harvested by centrifugation. Supernatant was discarded, and 60μL of B-Per (ThermoFisher Scientific) was added to each well. Cell pellets were simultaneously resuspended and lysed by shaking at room temperature for 20 minutes. Cell lysate was clarified by centrifugation and two aliquots of 25μL of supernatant containing soluble HsKYNase protein was transferred to 96-well plates pre-loaded with 25μL PBS. Plates were screened by adding 150μL of Kyn substrate in PBS pH 7.4 (either 500μM or 50μM Kyn concentration) and then monitoring absorbance at 365nm for 10 to 60 minutes. Specific activity was calculated in comparison to controls by analyse the slope of Kyn degradation by plotting time versus absorbance at 365nm.

Enzyme purification

Enzymes were expressed in BL21(DE3), C41(DE3), C41(DE3), T7 Express, or T7 ΔtrpE strains, as described previously [14,64]. Single colonies of *E. coli* were used to inoculate 3-ml starter cultures of LB antibiotic and grown overnight at 37 °C. 2.5 mL of the starter cultures was used to inoculate 500 mL of Terrific Broth + antibiotic, which were grown to an OD_{600} = 0.80 at 37 °C before induction with 0.5 μM IPTG (Fisher) at 25 °C and cultivation overnight. Cells were pelleted and resuspended in 25 ml lysis buffer, then lysed with a FRENCH Press cell disruptor (Thermo Electron Corporation) at 1,500 P.S.I.

Buffer formulations were as follows: Lysis buffer contained 100 mM sodium phosphate pH 8.0, 1 mM pyridoxal-5-phosphate monohydrate (PLP, Fisher), 300 mM NaCl, 1 mM phenylmethylsulfonyl fluoride (PMSF, Sigma), 25 mM imidazole (Fisher), 0.1% Tween 20 (Sigma) and 25 U/ml Universal Nuclease (Pierce); Wash buffer contained 300 mM NaCl, 100 mM sodium phosphate pH 8.0, 25 mM imidazole and 0.1% Tween 20; Elution buffer contained 300 mM NaCl, 100 mM sodium phosphate pH 8.0, 5 mM PLP, and 300 mM imidazole.

Following lysis, the solid fraction of the lysate was removed by a one hour centrifugation at 20,000*g*, then lysate supernatant was filtered with a 0.22-μm syringe filter and applied via gravity flow to a pre-equilibrated (with wash buffer) Ni-NTA (Qiagen) column. The column was washed with 20 column volumes of wash buffer, and then the enzyme was eluted with

5 column volumes of elution buffer. The eluant was incubated at 37 °C for 3 hours, dialyzed overnight at 4°C in 25 mM Tris-HCl pH 8.5, then buffer exchanged into DPBS.

The purification, PEGylation, and endotoxin removal processes for HsKYNase_95 prior to its use for *in vivo* mouse studies were performed as described previously [14].

Steady-state kinetic analyses

Michaelis–Menten kinetic parameters for KYNase enzymes against KYN (Sigma Aldrich) and 3-hydroxy-DL-kynurenine (OH-KYN, Sigma Aldrich) were determined using substrate concentrations ranging between 0mM and 2mM and enzyme concentrations ranging between 0.10 and 1.00 μM. Enzyme activity was gauged by monitoring decrease in KYN absorbance at 365 nm or OH-KYN absorbance at 373 nm over time. Initial reaction velocity per total enzyme concentration values were obtained from a linear regression of reaction progress curves with <10% of substrate degraded, and then plotted against substrate concentrations in KaleidaGraph (Synergy software). A nonlinear regression fitting the data to the Michaelis−Menten model (Equation 1) was used to calculate k_{cat} and K_M parameters. For determination of steady-state kinetic parameters of HsKYNase_66 in D_2O-PBS, the purified enzyme was buffer-exchanged against D_2O-PBS, pD=7.4. Substrates were prepared in D_2O-PBS and pD was adjusted to 7.0 for subsequent steady-state kinetic analysis.

$$v = (k_{cat} \times [S])/(K_M + S) \quad (1)$$

Pre-steady-state kinetic analyses

Pre-steady-state kinetic traces for the reaction of HsKYNase and HsKYNase_66 with KYN and OH-KYN were followed by stopped-flow fluorescence spectroscopy as described previously [15]. Briefly, for the reaction of each enzyme with KYN, the rate of formation of the first product anthranilic acid (AA) was measured by exciting at 314 nm and recording the emitted light at 393 nm using single band bandpass filters (Semrock, Rochester, NY). Similarly, the produced 3-hydroxy-anthranilic acid (OH-AA) during the reaction with OH-KYN was measured by exciting at 318 nm and detecting fluorescence at 407 nm. For the reaction with KYN, 5 μM of HsKYNase_66 was mixed with 500 μM substrate in the stopped-flow instrument (SF-300x instrument from KinTek Corporation) whereas for the reaction with OH-KYN, 12.5 μM HsKYNase_66 and 1000 μM OH-KYN were mixed, respectively. For the experiments with HsKYNase, 25 μM and 5 μM enzyme was mixed with 800 μM and 500 μM KYN and OH-KYN, respectively. All concentrations are final after mixing the enzyme with the respective substrate in the stopped-flow instrument. All reactions were performed at 37 °C in DPBS and in all plots each trace represents the average of five different reactions. The conversion of fluorescence signals to actual concentration of AA and OH-AA was done by generating standard curves upon mixing known concentrations of either AA or OH-AA in the stopped-flow apparatus and recording the fluorescence for each concentration. For the calculation of burst and linear rates, the data was analytically fit to a single-burst model described below (Equation 2) by non-linear regression using KinTek Explorer program.

$$Y = Ae^{(-k_{burst}\,t)} + k_{cat}t \quad (2)$$

where A is the amplitude, k_{burst} is the decay rate of the burst phase (eigenvalue) and k_{cat} is the steady-state turnover rate of the reaction.

Crystallization and structure determination of HsKYNase_66

Following nickel column purification and buffer exchange, HsKYNase_66-Ct6XHis (HsKYNase_66 with a C-terminal 6X-Histidine Tag) was dialyzed against a dialysis buffer consisting of 50 mM HEPES pH 8.0, 50 mM NaCl, 0.2 mM PLP solution for 6 hours at 4°C and further purified through gel filtration using a Sephadex 200 column (GE Healthcare) in dialysis buffer. HsKYNase_66_Ct6XHis was concentrated to a final concentration of 7.4 mg/mL using a Vivaspin Turbo 10,000 MWCO ultrafiltration unit prior to crystallization.

Diffracting crystals were obtained through vapor diffusion in sitting drops by mixing 1 part 7.4 mg/mL HsKYNase_66_Ct6XHis supplemented with 0.005 mg/mL trypsin (to remove any flexible terminal ends of the protein) with 1 part crystallization solution (8% PEG 8000, 100 mM imidazole, 50 mM $MgCl_2$, 0.2 mM PLP, and 5% sucrose) followed by incubation at 4°C. Well-formed crystals were cryo-protected in 30% D-xylitol, 6% PEG 8000, 0.1 M imidazole, 0.2 mM PLP and then flash frozen in liquid nitrogen prior to data collection.

X-ray diffraction data was collected at the Advanced Photon Source (APS) beamline 23ID-D (Argonne) and processed using the HKL 2000 software suite [65]. The structure was solved using molecular replacement in Phaser (Phenix) with the previously solved human kynureninase structure (PDB: 2HZP) as a search model [66,67]. Refinement of the initial model was accomplished through iterative model building in COOT [68]. Models were refined in Phenix with 5% of the diffraction set as a test for R_{free} cross-validation. Data collection and refinement statistics are summarized in Supplementary Table 3. Validation of the engineered kynureninase structure was determined through visual inspection of individual mutations with reference to the calculated electron density maps in COOT, and molecular figures of the different mutation sites were generated using the PyMOL Molecular Graphics System, Version 2.0 (Schrödinger, LLC). The HsKYNase_66 structure was deposited into the Worldwide Protein Data Bank with PDB code 7S3V.

HDX-MS

Experiments were performed as had been done in our prior work [15]. Flash-frozen HsKYNase_66 aliquot (>100 μM) was thawed on ice and incubated with 5 mM PLP at 37 °C for ~ 3 h. Labelling buffer was prepared by dissolving either KYN, 3-DL-OH-KYN, or no substrate in D_2O-1x PBS, pD 7.4 yielding a final concentration of 3.125 mM. Following the PLP incubation, a fraction of HsKYNase_66 was diluted 1:24 (v/v) with labelling buffer at a final concentration of 1.6 μM enzyme and 3 mM substrate in 1x PBS at 37 °C. Enzymes were labelled for 0, 1, 10, or 100 minutes. Each time course was repeated in triplicate with freshly prepared labelling buffer for both substrates. Labelling reactions were quenched 1:1 in 2 M GuHCl, 0.8% (v/v) formic acid at 1 °C, pH 2.6. The samples were injected

immediately or flash frozen and thawed prior to online pepsin digestion, trapping, and elution.

Liquid chromatography: A Waters M-Class coupled with HDX Manager (equipped with a 50 μL loop) was used to perform protein digestion followed by peptide trapping and elution. Buffers A and B consisted of 0.1% (v/v) formic acid and 0.1% (v/v) formic acid in 100% acetonitrile, respectively. An Enzymate Pepsin Column (Waters, 300 Å, 5 μm, 2.1 × 30 mm) was used for online digestion at 15 °C. Digestion and subsequent trapping were performed for 3 minutes at a flow of 100 μL/min. All peptides were desalted via reverse-phase trap (Waters Protein BEH C4 VanGuard Pre-column, 300 Å, 1.7 μm, 2.1 × 5 mm) and separated on a C18 column (Waters BEH C18 Column, 130 Å, 1.7 μm, 1 × 100 mm) at 1 °C using an isocratic gradient from 3–40% buffer B at 40 μL/min for 7 minutes. Following peptide digestion, a pepsin wash solution consisting of 2 M GuHCl, 4% ACN, 0.8% (v/v) formic acid, was injected to minimize carryover. Blank injections were performed after each sample injection to ensure that low carryover was maintained.

Mass spectrometry: All data was acquired in resolution mode on a Synapt G2-S*i* Q-TOF (Waters) using positive ion mode for either HDMS or HDMS^E modes. HDMS^E mode was used to collect low (6 V) and high energy (ramping 22 – 44 V) data-independent peptide fragmentation data for downstream identification. HDMS mode was used for low energy ion data for deuterated samples. Parameters were set as follows: sample sprayer capillary voltage at 2.8 kV, desolvation gas at 650 L/hour and 175 °C with source temperature of 80 °C, cone gas flow at 90 L/hour, nebulizer gas at 6.5 bar, and sampling cone and source offset at 30 V. The mass correction was performed with [Glu^1]-fibrinopeptide B as a reference mass, and data was acquired with a 0.4 second scan time and range of 100–2000 m/z.

HDX data analysis: Data analysis was employed by exporting the raw files to Protein Lynx Global Server 3.0.2 (Waters) for peptide identification. Low energy, high energy, and intensity thresholds were set to 250, 50, and 750 counts, respectively. Minimum fragment ion matches per peptide was set to 3. Peptide and fragment tolerances were both set to automatic whereas missed cleavages were set to 1 with false discovery rate of 4. PLGS peptide lists were exported to DynamX 3.0 (Waters) and used to locate peptides in raw files and assign their weighted relative uptake profiles. DynamX 3.0 thresholds were set to 0.3 Minimum products per amino acid and 1 Minimum consecutive product. File threshold was set to 3, utilizing peptide lists from a total of 6 controls. All other DynamX 3.0 parameters were left unmodified. All DynamX 3.0 results were manually verified and filtered by applying a Welch's t-test at 99% confidence to identify significant peptides using HD-eXplosion [69].

Standards and reagents: Ultrapure grade water was purchased from EMD Millipore, and analytical grade formic acid, methanol, acetonitrile, and dimethylsulfoxid were from Fisher Scientific. Calibration solutions were from Thermo Scientific. Deuterated standards were purchased from Cambridge Isotope Laboratories (CIL), Buchem, or Acros Organics as follows: 3-hydroxy-DL-kynurenine (5,8,8-D3, 98% purity, Buchem) and 3-hydroxyanthranilic acid (4,6-D2, 98% purity, Buchem), anthranilic acid (3,4,5,6-D4, 98%

purity, Buchem), Dl-glutamic acid (2,4,4-D3, 98% purity, CIL), fumaric acid (2,3-D2, 98% purity, CIL), kynurenic acid (3,4,6,7,8-D5, 98% purity, Buchem), kynurenine (D4, 98% purity, Buchem), L-tryptophan (indole-D5, 98% purity, CIL) nicotinic acid (D4, 98% purity, CIL), picolinic acid (99% purity, Acros), and quinolinic acid (4,5,6-D3, 99% purity, Buchem).

Differential Scanning Fluorimetry

A Lightcycler 480 instrument (Roche) and SYPRO Orange dye (Sigma) were used to determine melting temperature following the manufacturer's protocols, using a simultaneous titration of KYNase enzyme and dye ranging from 0.5–8μM of enzyme and 5x to 20x of SYPRO Orange. Analysis was performed using the LightCycler 480 Software and confirmed with visual inspection.

Mouse experiments

BALB/cJ mice from Jackson Laboratories (Bar Harbor, Maine, USA) were maintained at UT Austin or Ikena Oncology in pathogen-free, ventilated cages with irradiated food and autoclaved water. Institutional Animal Care and Use Committees at UT Austin or Ikena Oncology approved experimental procedures, and housing conditions for mice were as follows: 12 light/12 dark cycle, 65–75 degrees Fahrenheit temperature, and 40–60% relative humidity. Mice were monitored daily. Mice were euthanized by CO_2 asphyxiation and cervical dislocation at study endpoints or after showing signs of distress.

N = 8 mice per experimental arm were inoculated with 5×10^4 of CT26 cells in the flank, and treatments were started when tumour sizes reached 50–100 mm^3. of PEGylated-HsKynase_95 (20 mg/kg) or vehicle control was administered by peritumoral injections every three days, and 10mg/kg clone RMP1–14 anti-PD-1 antibody (Bio X Cell) was administered by intraperitoneal injection as described previously [14]. Tumour size was measured with callipers three times per week.

Statistical analysis

For statistical significance (P value) analysis, the data was first subjected to a Normality test to ensure that parametric statistics can be employed of the evaluation of the results. Subsequently, unpaired Student's t-test (two-tailed) were performed. Significant P value is denoted as *P<0.05. Statistical analyses were performed with GraphPad Prism.

Data availability

The datasets generated and/or analysed during the current study are attached, and additional data are available from the corresponding authors upon reasonable request. Source data for Figure 5 are attached, and the HsKYNase_66 structure was deposited into the Worldwide Protein Data Bank with PDB code 7S3V.

Supplementary Material

Refer to Web version on PubMed Central for supplementary material.

Acknowledgements

This work was supported by grants from the NIH 1 RO1 CA189623 (G.G. and E.S.), the Cancer Prevention Research Institute of Texas grant DP150061 (G.G. and E.S.), and Ikena Oncology (G.G. and E.S.), funding from the University of Texas System Proteomics network (S.D.), as well as grants R01GM104896 (Y.J.Z.) and R01GM125882 (Y.J.Z.) from the NIH and postdoctoral fellowships from the American Cancer Society - 128252-PF-15–143-01-CDD (J.B.) and grant 123506-PF-13–354-01-CDD (N.M.).

References

1. Opitz CA et al. An endogenous tumour-promoting ligand of the human aryl hydrocarbon receptor. Nature 478, 197–203 (2011). [PubMed: 21976023]
2. Cervenka I, Agudelo LZ & Ruas JL Kynurenines: Tryptophan's metabolites in exercise, inflammation, and mental health. Science 357, (2017).
3. Nguyen DJM et al. Targeting the Kynurenine Pathway for the Treatment of Cisplatin-Resistant Lung Cancer. Mol Cancer Res 18, 105–117 (2020). [PubMed: 31628200]
4. Frumento G et al. Tryptophan-derived catabolites are responsible for inhibition of T and natural killer cell proliferation induced by indoleamine 2,3-dioxygenase. J Exp Med 196, 459–468 (2002). [PubMed: 12186838]
5. Puccetti P et al. Accumulation of an endogenous tryptophan-derived metabolite in colorectal and breast cancers. PLoS One 10, e0122046 (2015). [PubMed: 25881064]
6. Holmgaard RB, Zamarin D, Munn DH, Wolchok JD & Allison JP Indoleamine 2,3-dioxygenase is a critical resistance mechanism in antitumor T cell immunotherapy targeting CTLA-4. J Exp Med 210, 1389–1402 (2013). [PubMed: 23752227]
7. Mezrich JD et al. An interaction between kynurenine and the aryl hydrocarbon receptor can generate regulatory T cells. J Immunol 185, 3190–3198 (2010). [PubMed: 20720200]
8. Prendergast GC, Malachowski WP, DuHadaway JB & Muller AJ Discovery of IDO1 inhibitors: from bench to bedside. Cancer Res 77, 6795–6811 (2017). [PubMed: 29247038]
9. Li H et al. The landscape of cancer cell line metabolism. Nat Med 25, 850–860 (2019). [PubMed: 31068703]
10. Röhrig UF, Majjigapu SR, Vogel P, Zoete V & Michielin O Challenges in the Discovery of Indoleamine 2,3-Dioxygenase 1 (IDO1) Inhibitors. J Med Chem 58, 9421–9437 (2015). [PubMed: 25970480]
11. Dounay AB, Tuttle JB & Verhoest PR Challenges and Opportunities in the Discovery of New Therapeutics Targeting the Kynurenine Pathway. J Med Chem 58, 8762–8782 (2015). [PubMed: 26207924]
12. Günther J, Däbritz J & Wirthgen E Limitations and Off-Target Effects of Tryptophan-Related IDO Inhibitors in Cancer Treatment. Front Immunol 10, (2019).
13. Jennings MR, Munn D & Blazeck J Immunosuppressive metabolites in tumoral immune evasion: redundancies, clinical efforts, and pathways forward. J Immunother Cancer 9, e003013 (2021). [PubMed: 34667078]
14. Triplett TA et al. Reversal of indoleamine 2,3-dioxygenase-mediated cancer immune suppression by systemic kynurenine depletion with a therapeutic enzyme. Nat Biotechnol 36, 758–764 (2018). [PubMed: 30010674]
15. Karamitros CS et al. Conformational Dynamics Contribute to Substrate Selectivity and Catalysis in Human Kynureninase. ACS Chem Biol 15, 3159–3166 (2020). [PubMed: 33275413]
16. Pokrovsky VS, Kazanov MD, Dyakov IN, Pokrovskaya MV & Aleksandrova SS Comparative immunogenicity and structural analysis of epitopes of different bacterial L-asparaginases. BMC Cancer 16, (2016).
17. Mayer A et al. Modifying an immunogenic epitope on a therapeutic protein: a step towards an improved system for antibody-directed enzyme prodrug therapy (ADEPT). Br J Cancer 90, 2402–2410 (2004). [PubMed: 15162148]
18. Trudeau DL & Tawfik DS Protein engineers turned evolutionists-the quest for the optimal starting point. Curr Opin Biotechnol 60, 46–52 (2019). [PubMed: 30611116]

19. Goldsmith M & Tawfik DS Enzyme engineering: reaching the maximal catalytic efficiency peak. Curr Opin Struct Biol 47, 140–150 (2017). [PubMed: 29035814]
20. Zakas PM et al. Enhancing the pharmaceutical properties of protein drugs by ancestral sequence reconstruction. Nat Biotechnol 35, 35–37 (2017). [PubMed: 27669166]
21. Thomas A, Cutlan R, Finnigan W, van der Giezen M & Harmer N Highly thermostable carboxylic acid reductases generated by ancestral sequence reconstruction. Commun Biol 2, 1–12 (2019). [PubMed: 30740537]
22. Merkl R & Sterner R Reconstruction of ancestral enzymes. Perspect Sci 9, 17–23 (2016).
23. Gumulya Y et al. Engineering highly functional thermostable proteins using ancestral sequence reconstruction. Nat Catal 1, 878–888 (2018).
24. Trifinopoulos J, Nguyen L-T, von Haeseler A & Minh BQ W-IQ-TREE: a fast online phylogenetic tool for maximum likelihood analysis. Nucleic Acids Res 44, W232–235 (2016). [PubMed: 27084950]
25. Bloom JD & Arnold FH In the light of directed evolution: Pathways of adaptive protein evolution. PNAS 106, 9995–10000 (2009). [PubMed: 19528653]
26. Tawfik DS Enzyme promiscuity and evolution in light of cellular metabolism. FEBS J 287, 1260–1261 (2020). [PubMed: 32250557]
27. Khersonsky O, Roodveldt C & Tawfik DS Enzyme promiscuity: evolutionary and mechanistic aspects. Curr Opin Chem Biol 10, 498–508 (2006). [PubMed: 16939713]
28. Leveson-Gower RB, Mayer C & Roelfes G The importance of catalytic promiscuity for enzyme design and evolution. Nat Rev Chem 3, 687–705 (2019).
29. Romero PA & Arnold FH Exploring protein fitness landscapes by directed evolution. Nat Rev Mol Cell Biol 10, 866–876 (2009). [PubMed: 19935669]
30. Bloom JD, Labthavikul ST, Otey CR & Arnold FH Protein stability promotes evolvability. PNAS 103, 5869 (2006). [PubMed: 16581913]
31. Firnberg E & Ostermeier M PFunkel: efficient, expansive, user-defined mutagenesis. PLoS One 7, e52031 (2012). [PubMed: 23284860]
32. Coco WM et al. DNA shuffling method for generating highly recombined genes and evolved enzymes. Nat Biotechnol 19, 354–359 (2001). [PubMed: 11283594]
33. Gupta RD & Tawfik DS Directed enzyme evolution via small and effective neutral drift libraries. Nat Methods 5, 939–942 (2008). [PubMed: 18931667]
34. Weinreich DM, Delaney NF, Depristo MA & Hartl DL Darwinian evolution can follow only very few mutational paths to fitter proteins. Science 312, 111–114 (2006). [PubMed: 16601193]
35. Tracewell CA & Arnold FH Directed enzyme evolution: climbing fitness peaks one amino acid at a time. Curr Opin Chem Biol 13, 3–9 (2009). [PubMed: 19249235]
36. Lima S, Kumar S, Gawandi V, Momany C & Phillips RS Crystal structure of the Homo sapiens kynureninase-3-hydroxyhippuric acid inhibitor complex: insights into the molecular basis of kynureninase substrate specificity. J Med Chem 52, 389–396 (2009). [PubMed: 19143568]
37. Wang S & Dai L Evolving generalists in switching rugged landscapes. PLoS Comput Biol 15, e1007320 (2019). [PubMed: 31574088]
38. Kvitek DJ & Sherlock G Reciprocal Sign Epistasis between Frequently Experimentally Evolved Adaptive Mutations Causes a Rugged Fitness Landscape. PLoS Genet 7, e1002056 (2011). [PubMed: 21552329]
39. Poelwijk FJ, Tănase-Nicola S, Kiviet DJ & Tans SJ Reciprocal sign epistasis is a necessary condition for multi-peaked fitness landscapes. J Theor Biol 272, 141–144 (2011). [PubMed: 21167837]
40. Yang G et al. Higher-order epistasis shapes the fitness landscape of a xenobiotic-degrading enzyme. Nat Chem Biol 15, 1120–1128 (2019). [PubMed: 31636435]
41. Lima S, Khristoforov R, Momany C & Phillips RS Crystal structure of Homo sapiens kynureninase. Biochemistry 46, 2735–2744 (2007). [PubMed: 17300176]
42. Momany C, Levdikov V, Blagova L, Lima S & Phillips RS Three-dimensional structure of kynureninase from Pseudomonas fluorescens. Biochemistry 43, 1193–1203 (2004). [PubMed: 14756555]

43. Wales TE & Engen JR Hydrogen exchange mass spectrometry for the analysis of protein dynamics. Mass Spectrom Rev 25, 158–170 (2006). [PubMed: 16208684]
44. Toh JWT et al. The Potential Value of Immunotherapy in Colorectal Cancers: Review of the Evidence for Programmed Death-1 Inhibitor Therapy. Clin Colorectal Cancer 15, 285–291 (2016). [PubMed: 27553906]
45. Labadie BW, Bao R & Luke JJ Reimagining IDO Pathway Inhibition in Cancer Immunotherapy via Downstream Focus on the Tryptophan–Kynurenine–Aryl Hydrocarbon Axis. Clin Cancer Res 25, 1462–1471 (2019). [PubMed: 30377198]
46. Hawkins DS et al. Asparaginase pharmacokinetics after intensive polyethylene glycol-conjugated L-asparaginase therapy for children with relapsed acute lymphoblastic leukemia. Clin Cancer Res 10, 5335–5341 (2004). [PubMed: 15328169]
47. Guttmann A, Krasnokutsky S, Pillinger MH & Berhanu A Pegloticase in gout treatment - safety issues, latest evidence and clinical considerations. Ther Adv Drug Saf 8, 379–388 (2017). [PubMed: 29204266]
48. Aharoni A et al. The 'evolvability' of promiscuous protein functions. Nat Genet 37, 73–76 (2005). [PubMed: 15568024]
49. Soskine M & Tawfik DS Mutational effects and the evolution of new protein functions. Nat Rev Genet 11, 572–582 (2010). [PubMed: 20634811]
50. Buller AR et al. Directed Evolution Mimics Allosteric Activation by Stepwise Tuning of the Conformational Ensemble. J Am Chem Soc 140, 7256–7266 (2018). [PubMed: 29712420]
51. Liang Z-X, Tsigos I, Bouriotis V & Klinman JP Impact of Protein Flexibility on Hydride-Transfer Parameters in Thermophilic and Psychrophilic Alcohol Dehydrogenases J Am Chem Soc 126, 9500–9501 (2004). [PubMed: 15291528]
52. Pabis A, Risso VA, Sanchez-Ruiz JM & Kamerlin SC Cooperativity and flexibility in enzyme evolution. Curr Opin Struct Biol 48, 83–92 (2018). [PubMed: 29141202]
53. Klinman JP Dynamically Achieved Active Site Precision in Enzyme Catalysis. Acc Chem Res 48, 449–456 (2015). [PubMed: 25539048]
54. Nestl BM & Hauer B Engineering of Flexible Loops in Enzymes. ACS Catal 4, 3201–3211 (2014).
55. Zhang J, Balsbaugh JL, Gao S, Ahn NG & Klinman JP Hydrogen deuterium exchange defines catalytically linked regions of protein flexibility in the catechol O-methyltransferase reaction. PNAS 117, 10797–10805 (2020). [PubMed: 32371482]
56. Campbell E et al. The role of protein dynamics in the evolution of new enzyme function. Nat Chem Biol 12, 944–950 (2016). [PubMed: 27618189]
57. González MM, Abriata LA, Tomatis PE & Vila AJ Optimization of Conformational Dynamics in an Epistatic Evolutionary Trajectory. Mol Biol Evol 33, 1768–1776 (2016). [PubMed: 26983555]
58. Ramanathan A & Agarwal PK Evolutionarily Conserved Linkage between Enzyme Fold, Flexibility, and Catalysis. PLOS Biology 9, e1001193 (2011). [PubMed: 22087074]
59. Otten R et al. How directed evolution reshapes the energy landscape in an enzyme to boost catalysis. Science 370, 1442–1446 (2020). [PubMed: 33214289]
60. Molineux G Pegylation: engineering improved pharmaceuticals for enhanced therapy. Cancer Treat Rev 28, 13–16 (2002). [PubMed: 12173407]
61. Vita R et al. The Immune Epitope Database (IEDB): 2018 update. Nucleic Acids Res 47, D339–D343 (2019). [PubMed: 30357391]
62. Deboer HA, Comstock LJ & Vasser M The Tac promoter - A functional hybrid derived from the Trp and Lac promoters. PNAS 80, 21–25 (1983). [PubMed: 6337371]
63. Thomason L, Costantino N & Court D *E. coli* Genome Manipulation by P1 Transduction. Curr Protoc Mol Biol 79, 1.17.1–1.17.8 (2007).
64. Miroux B & Walker JE Over-production of proteins in Escherichia coli: Mutant hosts that allow synthesis of some membrane proteins and globular proteins at high levels. J Mol Biol 260, 289–298 (1996). [PubMed: 8757792]
65. Otwinowski Z & Minor W Processing of X-ray diffraction data collected in oscillation mode. Methods Enzymol 276, 307–326 (1997). [PubMed: 27754618]

66. Adams PD et al. PHENIX: a comprehensive Python-based system for macromolecular structure solution. Acta Crystallogr D 66, 213–221 (2010). [PubMed: 20124702]

67. McCoy AJ et al. Phaser crystallographic software. J Appl Crystallogr 40, 658–674 (2007). [PubMed: 19461840]

68. Emsley P, Lohkamp B, Scott WG & Cowtan K Features and development of Coot. Acta Crystallogr D 66, 486–501 (2010). [PubMed: 20383002]

69. Zhang N, Yu X, Zhang X & D'Arcy S HD-eXplosion: visualization of hydrogen-deuterium exchange data as chiclet and volcano plots with statistical filtering. Bioinformatics 37, 1926–1927 (2021). [PubMed: 33079991]

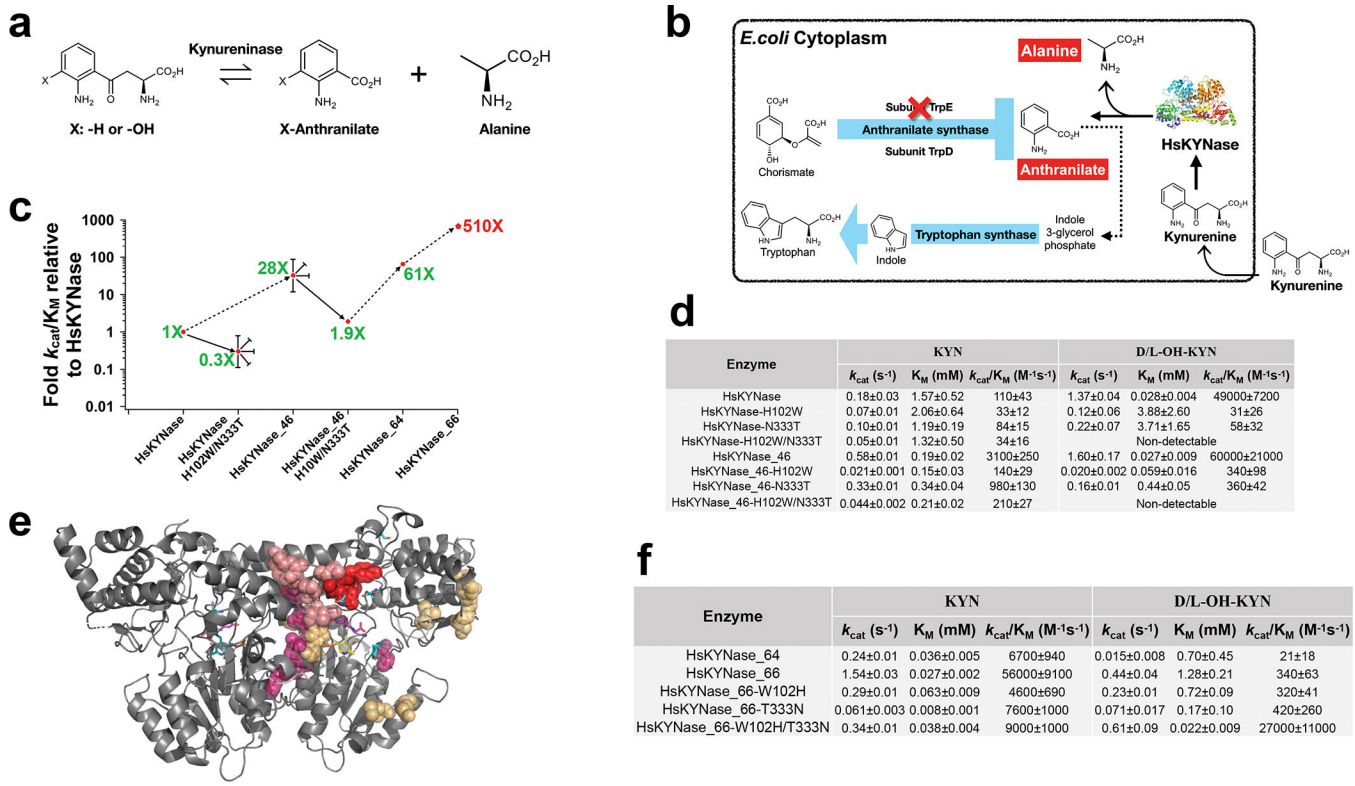

d

Enzyme	KYN			D/L-OH-KYN		
	k_{cat} (s^{-1})	K_M (mM)	k_{cat}/K_M ($M^{-1}s^{-1}$)	k_{cat} (s^{-1})	K_M (mM)	k_{cat}/K_M ($M^{-1}s^{-1}$)
HsKYNase	0.18±0.03	1.57±0.52	110±43	1.37±0.04	0.028±0.004	49000±7200
HsKYNase-H102W	0.07±0.01	2.06±0.64	33±12	0.12±0.06	3.88±2.60	31±26
HsKYNase-N333T	0.10±0.01	1.19±0.19	84±15	0.22±0.07	3.71±1.65	58±32
HsKYNase-H102W/N333T	0.05±0.01	1.32±0.50	34±16	Non-detectable		
HsKYNase_46	0.58±0.01	0.19±0.02	3100±250	1.60±0.17	0.027±0.009	60000±21000
HsKYNase_46-H102W	0.021±0.001	0.15±0.03	140±29	0.020±0.002	0.059±0.016	340±98
HsKYNase_46-N333T	0.33±0.01	0.34±0.04	980±130	0.16±0.01	0.44±0.05	360±42
HsKYNase_46-H102W/N333T	0.044±0.002	0.21±0.02	210±27	Non-detectable		

f

Enzyme	KYN			D/L-OH-KYN		
	k_{cat} (s^{-1})	K_M (mM)	k_{cat}/K_M ($M^{-1}s^{-1}$)	k_{cat} (s^{-1})	K_M (mM)	k_{cat}/K_M ($M^{-1}s^{-1}$)
HsKYNase_64	0.24±0.01	0.036±0.005	6700±940	0.015±0.008	0.70±0.45	21±18
HsKYNase_66	1.54±0.03	0.027±0.002	56000±9100	0.44±0.04	1.28±0.21	340±63
HsKYNase_66-W102H	0.29±0.01	0.063±0.009	4600±690	0.23±0.01	0.72±0.09	320±41
HsKYNase_66-T333N	0.061±0.003	0.008±0.001	7600±1000	0.071±0.017	0.17±0.10	420±260
HsKYNase_66-W102H/T333N	0.34±0.01	0.038±0.004	9000±1000	0.61±0.09	0.022±0.009	27000±11000

Figure 1. Directed evolution of HsKYNase and development of a KYN specialist variant.

a, Reactions catalysed by kynureninases. **b**, *E. coli* genetic selection scheme for isolation of high catalytic activity HsKYNase variants from large libraries. **c**, Schematic showing the directed evolution trajectory leading to the isolation of HsKYNase_66. Blunted arrows denote dead-end evolutionary intermediates, from which higher catalytic activity variants could not be selected from numerous libraries. **d**, Steady-state kinetic parameters of HsKYNase, HsKYNase_46 and their H102W, N333T or H102W/N333T variants with KYN and OH-KYN. Best fit value ± error for one representative measurement shown. **e**, Diagram of mutational strategies to overcome HsKYNase_46 evolutionary dead-end. Gray ribbon (entire protein sequence): denotes sites targeted by whole gene scanning saturation mutagenesis libraries, by EpPCR and in neutral drift selections, and by *in silico* designs. Right half of image shows HsKYNase_46 mutations as blue sticks, and amino acid residues targeted for mutagenesis in 2 (orange), 4–6 (dark pink), 8–9 (light pink), or 10 (red spheres) additional different libraries. **f**, Steady-state kinetic parameters of HsKYNase_64 and HsKYNase_66 as in **d** above.

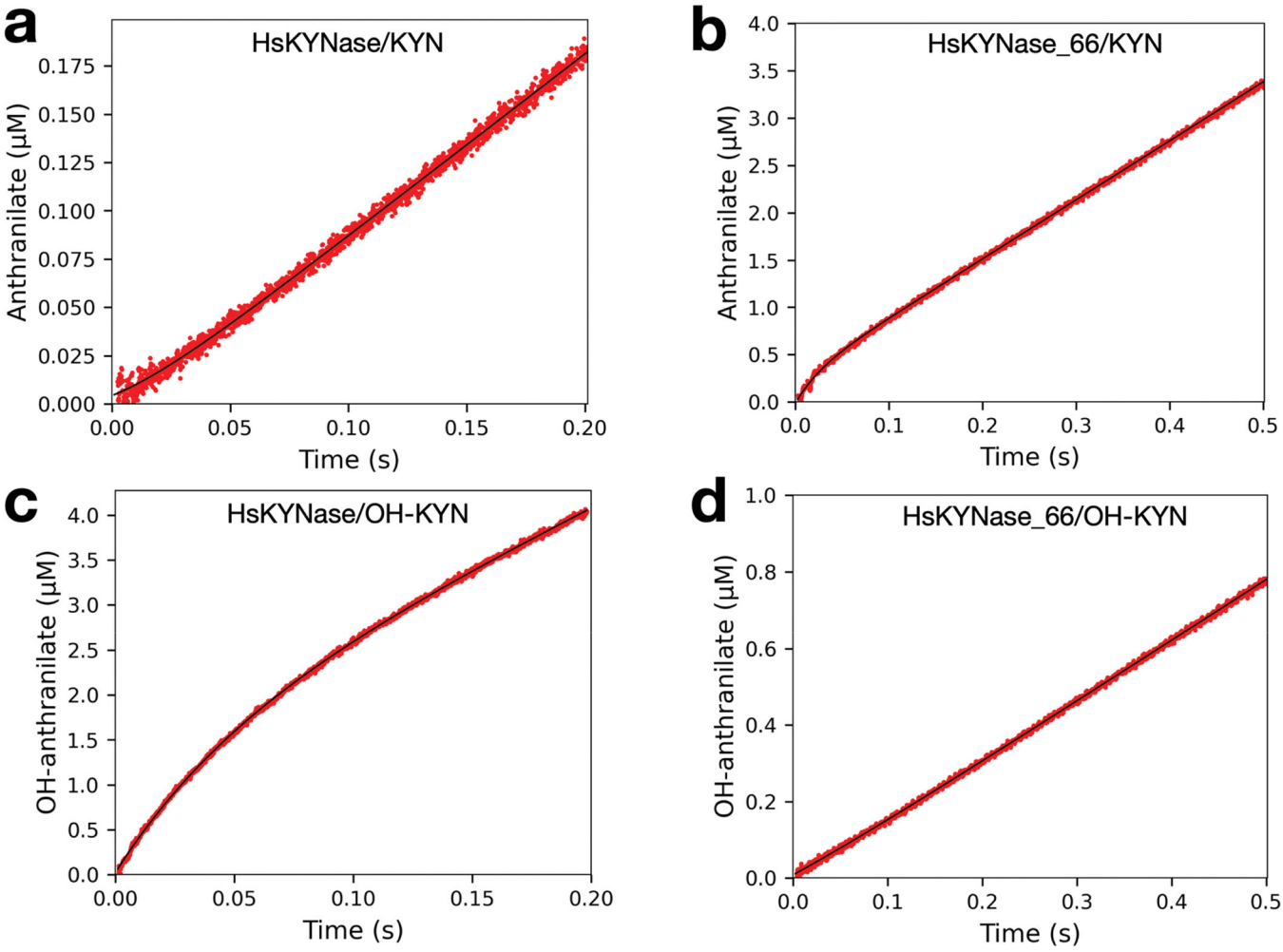

Figure 2. Pre-steady-state kinetic analysis.

Stopped flow, pre-steady state fluorescent trace of (OH-)anthranilate (first product of the reaction) formation with: **a**, 25μM HsKYNase with 800 μM KYN. **b**, 5 μM HsKYNase_66 with 500 μM KYN. **c**, 5 μM HsKYNase with 500 μM DL-3'-OH-KYN. **d**, 12.5 μM HsKYNase_66 with 1000 μM DL-3'-OH-KYN. Each trace represents the average of five different experiments. Red traces: data points; black line: fit to 1-exponential burst equation (Equation 2 in Methods).

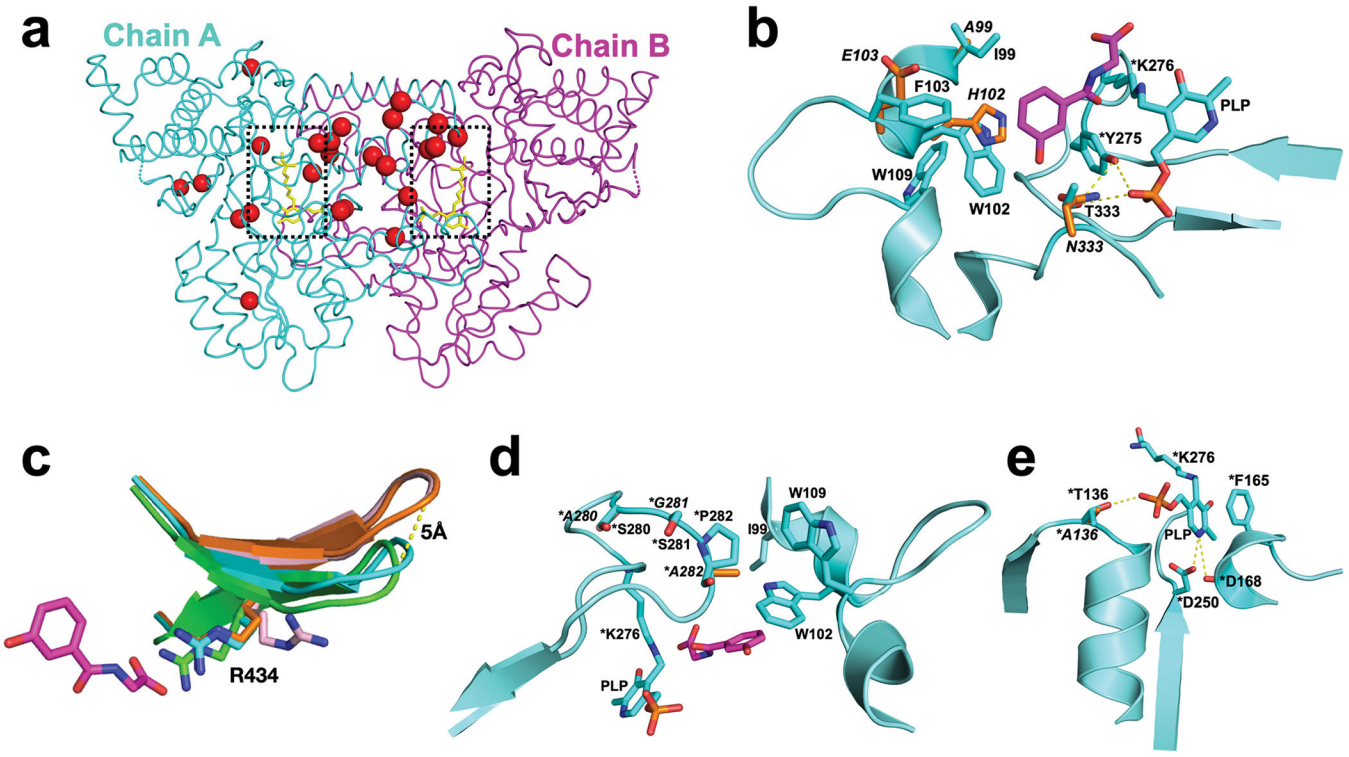

Figure 3. Crystal structure of HsKYNase_66 and its comparison to HsKYNase.

a, Loop cartoon representation of HsKYNase_66 crystal structure. Mutations are shown as red spheres and the PLP co-factor is shown as yellow sticks. Omit maps for selected mutations and PLP can be seen in Supplementary Fig. 6. **b**, Zoomed snapshot of HsKYNase_66 active site (PDB: 7S3V, cyan) overlaid against the structure of HsKYNase (PDB: 3E9K, orange) in complex with 3-hydroxyhippuric acid inhibitor (magenta). Where side chains are shown, C is cyan in HsKYNase_66 and orange in HsKYNase, N is blue, O is red, and P is orange). **c**, Zoomed-in overlay of the R428-R434 loop of substrate free HsKYNase_66 (PDB: 7S3V, cyan), HsKYNase (PDB: 3E9K, orange) in complex with 3-hydroxyhippuric acid inhibitor (magenta), substrate free HsKYNase (PDB: 2HZP, pink), and substrate free PfKYNase (PDB: 1QZ9, green) showing the different conformation of the R434 side chain for the open (2HZP, pink) verse closed (all others) KYNase conformations and shift of the loop itself in PfKYNase and HsKYNase_66 compared to HsKYNase. **d**, Zoom-in of the mutated SSP (A280S-G281S-A282P) active site loop in HsKYNase_66 and its location relative to I99, W102 and W109 residues as well as to the internal aldimine moiety and the substrate binding pocket (shown with 3-hydroxyhippuric acid inhibitor aligned from 3E9K). **e**, PLP binding pocket of HsKYNase_66. Asterisks indicate residues are contributed from the second chain relative to the chain that harbours the W102-T333 motif. Bold, italic labels show HsKYNase amino acid residues that are mutated in HsKYNase_66.

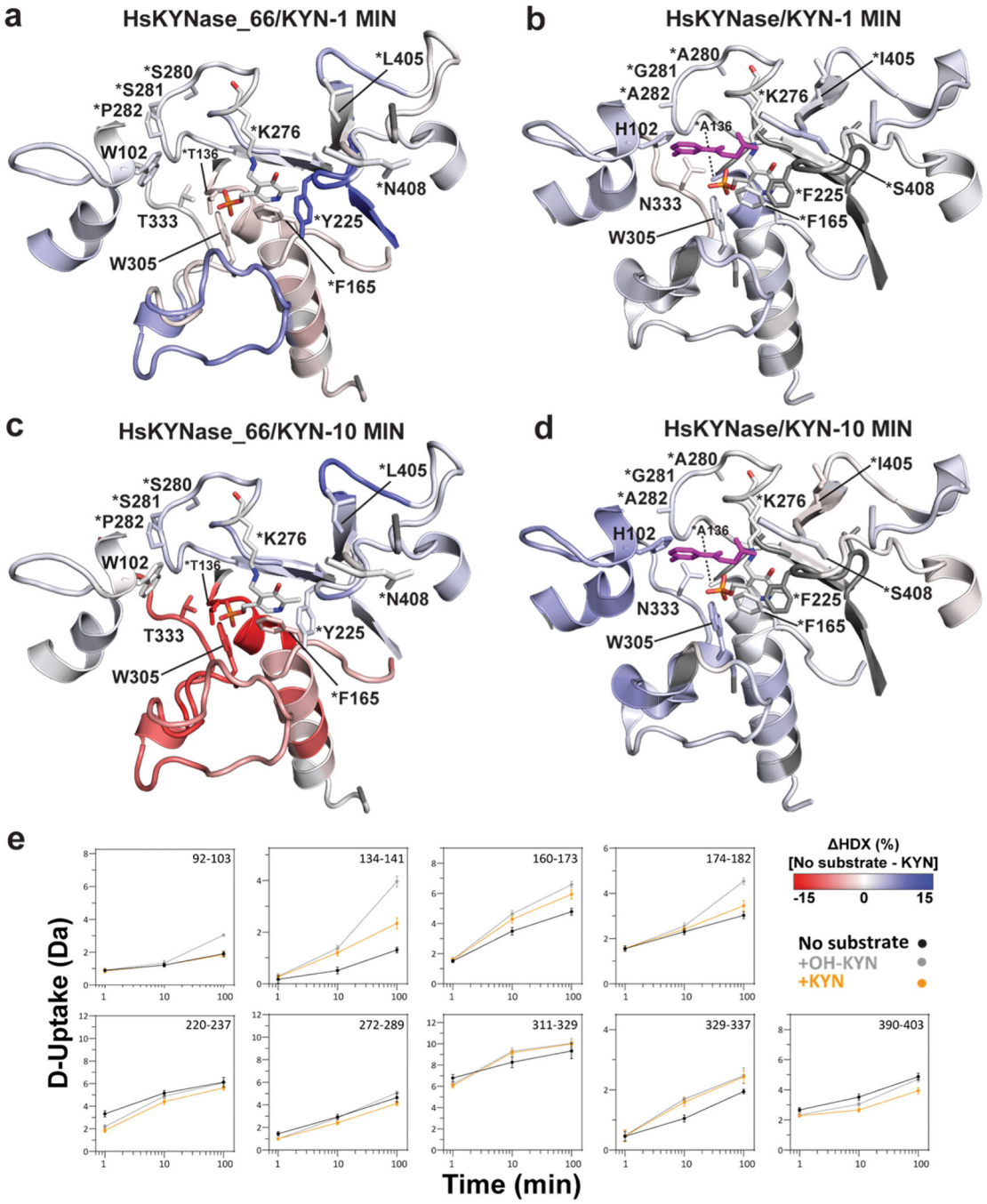

Figure 4. HDX-MS of HsKYNase_66 and HsKYNase in the reaction with KYN.

a-b, Zoom-in on the active site of HsKYNase_66 (PDB: 7S3V) and HsKYNase (PDB: 3E9K) respectively, coloured by the difference in fractional D-uptake (−15 to +15%) between no substrate and with KYN after 1 minute exposure to deuterium (data for HsKYNase are from [15]). Mutations (W102, *T136, *Y225, *S280, *S281, *P282, T333, *L405 and *N408) and important PLP-interacting residues (*F165, *K276, W305) of HsKYNase_66 located at regions with significant exchange are labelled. Asterisk indicates that residue is contributed by the “second” KYNase chain. The respective structurally

equivalent residues in case of HsKYNase are shown in panel b. Regions with significant exchange were determined based on overlapping peptides and assuming complete back-exchange of the N-terminal residue. Cut-offs for peptide significance are p <0.01 (determine by Welch's test) and average |ΔHDX|≥0.3. Residues without coverage are shown in grey. PLP is shown as sticks and coloured by atom (C is white, N is blue, O is red, and P is orange) while 3-hydroxyhippuric competitive inhibitor is shown in magenta sticks. Data shown as a volcano plot in Supplementary Fig. 13. **c-d,** Zoom-in on the active site of HsKYNase_66 and HsKYNase respectively, coloured by the difference in fractional D-uptake (−15 to +15%) between no substrate and with KYN after 10 minutes exposure to deuterium. **e**, D-uptake plots of HsKYNase_66 reaction with KYN and OH-KYN. Volcano plot for HsKYNase_66/OH-KYN reaction also shown in Supplementary Fig. 13. No substrate: black; with KYN: orange; with OH-KYN:grey. The Y-axis range scaled to 70% of max D-uptake assuming the N-terminal residue undergoes complete back-exchange. Error bars are ±2σ from three technical replicates. Abbreviations: HDX-MX - Hydrogen-Deuterium Exchange Mass Spectrometry; KYN - L-kynurenine; OH-KYN - 3'-OH-L-kynurenine.

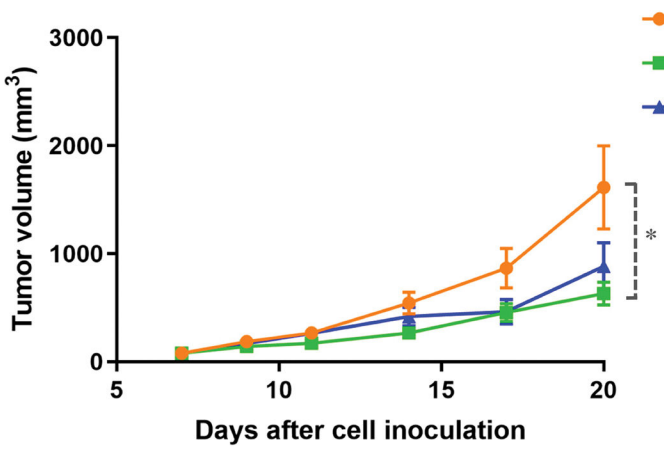

Enzyme	$(k_{cat}/K_M)_{KYN}$ ($M^{-1}s^{-1}$)	Activity after	
		3 hr	24 hr
Hs-Kynase_66	56000	22	0
Hs-Kynase_95	55000	44	1.8

Figure 5. Anti-tumour activity of an engineered human KYNase enzyme.

Time course of CT26 colon carcinoma tumour volumes treated with either vehicle, HsKYNase_95 or anti-PD-1 antibody. N = 8 mice for each experimental arm. Data are represented as mean ± s.e.m., and statistical significance was determined by an unpaired t-test (two-tailed). *P<0.05 comparing HsKYNase_95 treatment to vehicle control. The inset shows steady-state kinetic parameters and residual activity after incubation in serum for HsKYNase_66 and HsKYNase_95.

Table 1:

HsKYNase Variants of Interest

							% Stability in serum	
Enzyme	**# Mutations**	**List of Amino Acid Mutations**	**$k_{cat}(s^{-1})$**	**K_M(mM)**	**k_{cat}/K_M ($M^{-1}s^{-1}$)**	**Fold HsKYNase**	**After 3 hours**	**After 24 hours**
HsKYNase	0	N/A	0.18	1.57	110	1	17	2.7
HsKYNase_46	9	N67D/L72N/E103Q/ M189I/F225Y/S274G/ I331V/I405L/S408N	0.58	0.19	3100	28	0	0
HsKYNase_64	18	N67D/L72N/A99I/H102W/ E103F/V104E/K106E/ R107S/I110M/A136T/ M189I/F225Y/S274G/ I331C/N333T/S341I/ I405L/S408N	0.24	0.036	6700	61	0	0
HsKYNase_66	24	N67D/L72N/A99I/H102W/ E103F/V104E/K106D/ R107S/T111H/G112Y/ A132V/A136T/M189I/ V223I/F225Y/S274G/ A280S/G281S/A282P/ I331C/N333T/S341I/ I405L/S408N	1.54	0.027	56000	510	22	0
HsKYNase_95	25	N67D/A68T/L72N/A99I/ H102W/E103F/V104E/ K106D/R107S/I110L/ T111H/G112Y/A136T/ M189I/F225Y/S274N/ A280S/G281S/A282P/ F306W/I331C/N333T/ S341I/I405L/S408N	0.85	0.016	55000	500	44	1.8